ELECTRON SPIN RESONANCE IN DIAMOND

By

MARVIN DRAKE BELL

Bachelor of Science
Oklahoma State University
Stillwater, Oklahoma
1955

Master of Science
Oklahoma State University
Stillwater, Oklahoma
1956

Submitted to the Faculty of the Graduate School of
the Oklahoma State University
in partial fulfillment of the requirements
for the degree of
DOCTOR OF PHILOSOPHY
May, 1964

ELECTRON SPIN RESONANCE IN DIAMOND

Thesis Approved:

William J. Lewis
Thesis Adviser

H. E. Harrington

E. E. Kohnke

Tom E. Moore

F. C. Todd

J. H. Boggs
Dean of the Graduate School

ACKNOWLEDGMENTS

The author would like to express his sincere gratitude to Professor W. J. Leivo for his guidance, help, and constant encouragement during the course of this investigation.

Many other people have influenced and aided the present work, particular thanks are extended to Dr. H. E. Harrington, Dr. F. C. Todd, Dr. E. E. Kohnke, and Dr. T. E. Moore.

The semiconducting diamonds used in the investigation were kindly made available by Dr. J. F. H. Custers of the Diamond Research Laboratory, Dr. G. Switzer of the U. S. National Museum, and H. J. Stein of the Sandia Corporation. The author would like to express his appreciation to Dr. Custers for his continued interest and assistance in the diamond research at Oklahoma State University.

My association with all those connected with the research on diamonds has been rewarding. The help of members of the Physics-Chemistry shop in the design and construction of various components connected with the ESR spectrometer was greatly appreciated.

Finally, the financial support administered through the Research Foundation of Oklahoma State University and made available by the U.S. Air Force Office of Scientific Research and the National Science Foundation is greatfully acknowledged.

TABLE OF CONTENTS

LIST OF TABLES

LIST OF FIGURES

CHAPTER I

INTRODUCTION

Preliminary Remarks

The occurrence of natural semiconducting diamond and the growth of synthetic diamonds has greatly increased the interest shown in this material that is usually found to be an insulator with a large energy gap (5.5 eV). Silicon and germanium, both of which crystallize into the diamond structure, have received extensive theoretical and experimental investigations resulting in the existence of detailed information about the electronic energy level structure of these semiconductors. In contrast, the exact nature of energy levels in diamond remains incomplete although considerable information has been obtained on natural diamonds. The basic difference concerning the state of knowledge lies in the fact that impurities in diamond are extremely difficult to control when grown synthetically, and natural diamond may contain numerous unknown impurities or imperfections in varying concentrations. Therefore, in order to obtain a reasonably accurate and detailed knowledge of the energy levels in diamond, it is necessary to make an analysis using several different methods that can determine the parameters that give information concerning the electronic levels.

Electron spin resonance (ESR)[1] is one of the many methods that has contributed considerable information toward the understanding of the electronic energy levels of defects within semiconductors (1). It is advantageous to investigate the paramagnetism of semiconductors by the ESR method from several aspects. First, ESR absorption can be observed only if an unpaired spin is associated with the defect. This allows paramagnetic impurities to be detected in the presence of other types of impurities or imperfections that do not possess an unpaired electron. Second, very minute amounts of impurities can be detected because of the high sensitivity of the method. Third, hyperfine interaction may allow the identification of the impurity nucleus with which the unpaired electron is associated.

The purpose of the present research is to investigate the electronic energy level structure associated with defects in diamond through the application of the electron spin resonance method. The study will also include a review of the theory of magnetic resonance and the development of experimental techniques for the determination of the ESR parameters associated with the observed spectra in diamond.

Basic Ideas in Electron Spin Resonance

As previously mentioned, electron spin resonance is useful only when unpaired electrons are present in the solid under investigation. In the formation of various substances the chemical bonds result in the pairing of electron spins, such as the filling of electronic shells in the ionic

---

[1]Electron spin resonance is usually referred to as ESR for brevity. This notation will be adopted and used where appropriate.

bond or the sharing of electrons in the covalent bond (2). Therefore, most solids are diamagnetic and will contain no unpaired electrons unless defects are introduced into the lattice in the form of impurities or imperfections. Electron spin resonance can be observed in such systems as donor and acceptors in semiconductors, color centers in the alkali halides, free radicals, irradiated materials, chemical reactants, charred organic substances (such as dextrose), and carbon black (1, 3, 4).

The electron spin resonance phenomena can be initially discussed by considering the simple system in which an unpaired electron is associated with an atom or ion within a solid. Before the external magnetic field is applied the unpaired electrons will have the same energy, i.e., the energy levels in zero magnetic field are degenerate in electron spin. Upon application of the external magnetic field the degeneracy will be removed and each degenerate level will split into two levels. Classically this means that in a magnetic field the unpaired spins are oriented either parallel or antiparallel to the applied magnetic field. The interaction energy between the spin center having a magnetic moment $\vec{\mu}$ and the magnetic field $\vec{H}$ is given by $-\vec{\mu}\cdot\vec{H}$; hence, the Hamiltonian of the system is of the form

$$[H] = -\vec{\mu}\cdot\vec{H} \tag{1.1}$$

or using the relation $\vec{\mu} = -\gamma\hbar\vec{S}$ in (1.1) we have

$$[H] = \gamma\hbar\vec{S}\cdot\vec{H} \tag{1.2}$$

where γ is the gyromagnetic ratio, $\hbar$ is Planck's constant divided by 2π, and $\hbar\vec{S}$ is the electron spin operator. For a magnetic field, H_o, applied in the z-direction

$$[H] = \gamma\hbar H_o S_z \tag{1.3}$$

The eigenvalues of $\hbar S_z$ for this simple case are $\pm\frac{1}{2}\hbar$, and the energy levels of the unpaired electrons in the magnetic field are given by

$$E_{\pm} = \pm\tfrac{1}{2}\gamma\hbar H_o \tag{1.4}$$

with an energy separation

$$\Delta E = \gamma\hbar H_o \tag{1.5}$$

Figure 1-1 shows the energy levels of the unpaired electron in a static magnetic field. The + sign denotes the case when the spin is oriented parallel to the magnetic field. It should be noted that the magnetic moment $\vec{\mu}$ is oriented opposite to the spin vector $\vec{S}$ because γ is negative for the electron.

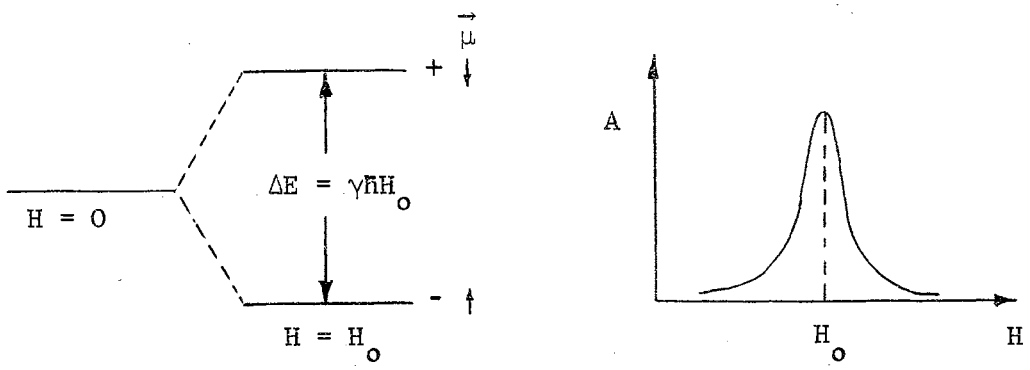

Figure 1-1. The energy levels of the unpaired electron are separated in a magnetic field by $\Delta E = \gamma\hbar H_o$. When the resonance condition $\omega = \gamma H_o$ is satisfied the electron system will absorb energy from the microwave field.

Radiation of energy ΔE can cause transitions between the parallel and the antiparallel orientations, i.e., cause a "spin flip". From the classical point of view, as will be discussed in chapter II, the magnetic moment vector precesses about the direction of the applied magnetic field with an angular frequency $\omega = \gamma H_o$, so that the frequency of precession is seen to correspond to the frequency of the radiation required for a spin flip. This is the resonance phenomena which, for electrons, usually involves a

frequency lying in the x-band region of the microwave spectrum and requiring magnetic fields of several thousand gauss. In ESR the g-factor is of primary importance and is defined by the expression

$$g = \frac{\sqrt{\mathcal{M}}}{\beta} \tag{1.6}$$

where β is the Bohr magneton $\frac{e\hbar}{2mc}$. Using equations (1.6) and (1.5) the fundamental equation for electron spin resonance takes the form

$$h\upsilon = g\beta H \tag{1.7}$$

where $\upsilon = \frac{\omega}{2\pi}$ is the microwave frequency. The deviation of the g- factor from the free electron value of 2.0023 is a measure of the orbital contribution to the magnetic moment.

The spin system is assumed to be in thermal equilibrium before the microwave magnetic field is applied with the equilibrium distribution of the spins between the two levels given by the Boltzmann expression,

$$\frac{n_+}{n_-} = \exp\ \frac{-\Delta E}{kT} \tag{1.5}$$

where n_+ is the number in the upper level, n_- is the number in the lower level, k is Boltzmann's constant, and T is the absolute temperature. Under the condition of equilibrium a net absorption of energy can occur until the two levels become equally populated. Two equally populated spin levels result in just as many spins taking part in stimulated emission as there are in absorption and, consequently, no resultant energy absorption takes place. Thus, if a net absorption of energy from the microwave field is to continue the system of spins must be in thermal equilibrium. Spin-lattice relaxation is one mechanism by which thermal equilibrium can be re-established. Coupling between the lattice and the spin system results in the spins losing energy to the lattice and a restoration of thermal equilibrium. This form of relaxation process is characterized by a "spin-lattice

relaxation time". Long spin-lattice relaxation times indicate weak coupling to the lattice, short times to strong coupling. For long spin-lattice relaxation times sufficient microwave power can be introduced to cause "saturation" of the resonance line.

In addition to the external magnetic field the unpaired electron may be associated with a nucleus possessing a magnetic moment. Thus, the electron will see an internal field due to the magnetic moment of the nucleus. There will be an interaction between the unpaired electron and the nucleus and the simple energy levels will split into several components depending on the spin of the nucleus. For a nucleus of spin I there will be $(2I + 1)$ component levels. A simple example can be given for $I = 1/2$. For such a nucleus there are two possible orientations; hence, the electron will see a magnetic field slightly greater and one slightly less than the applied field. The electronic levels will split into two components and ESR absorption will show two peaks. This hyperfine interaction allows the possibility of identifying the nucleus around which the electron moves, and the magnitude of the hyperfine splitting yields information regarding the interacting nucleus and the extent of the electronic orbit.

The simple picture of an unpaired electron, even including the hyperfine interaction, can be further complicated by crystalline field effects resulting in fine structure, and quadrapole interactions.

Some Properties of Diamond

Classification of and Impurities in Diamond

Diamonds have been classified into two principal types depending primarily on their infrared and ultraviolet absorption spectra (5). Type I diamonds have a rapidly increasing absorption coefficient for wavelengths

shorter than 3300Å and infrared absorption bands occurring in the 3-6μ and 6-13μ regions. Type II diamonds do not absorb strongly in the ultraviolet until the wavelength is near 2200Å and, in general, show no absorption in the 6-13μ region of the infrared, although the 3-6μ absorption bands due to lattice vibrational modes remain the same as in Type I.

This simple separation of diamond into two kinds is not completely satisfactory, and additional information concerning the optical absorption and other physical properties has been found useful in describing defect centers in diamond. Type I diamonds show infrared bands corresponding to different absorption centers. Two of these centers have been designated A and B; the infrared bands being correlated with observed absorption in the ultraviolet near the region of optical cut-off (6,7).

Group A

Infrared absorption peaks: 7.8, 8.3, 9.1, and 20.8μ.

Ultraviolet: Cut-off wavelength moves to longer wavelength and intensity of 3155Å line increases with increasing infrared absorption.

Group B

Infrared absorption peaks: 7.0, 7.3, 7.5, 8.5, 10, 12.9, and 30.5μ.

Ultraviolet: Correlated with 4155Å line intensity which is the origin of the blue fluorescence.

Nitrogen has been found to be present in Type I diamonds in a high concentration (8). A linear relationship was found between the nitrogen concentration and the infrared absorption at 7.8μ. From this work nitrogen was considered to enter the diamond lattice substitutionally and give rise to C-N molecular vibrations resulting in the group A bands. However, there has been some question as to the exact nature of the nitrogen defect

structure in diamond (16, 17, 18). Another impurity, manganese, has been attributed to the optical absorption at 5500Å resulting in mauve or pink diamonds (9, 29). The absorption due to manganese has been found to occur in some brown diamonds.

The apparent absence of the group A and group B bands in Type II diamonds indicates that the impurities or imperfections (or aggregates of these defects) are radically different than in Type I. The investigations of Custers (10, 11, 12) provided information leading to a further division and characterization of diamonds belonging to the Type II classification. Such unusual properties as a phosphorescence showing maxima at 4665, 5310, and 5720Å when excited with ultraviolet light of short wavelengths, and semiconductivity led to the subdivision of Type II diamonds into IIa and IIb categories. Type IIb diamonds are semiconductors and show characteristic absorption in the infrared at 1.85, 2.35, 2.43, 3.40, 3.56, 4.07, and 4.23μ that does not occur in insulating diamonds of Type I and IIa (7, 13).

Semiconducting diamonds are usually blue (12); the blue being due to optical absorption in the red and near infrared (14). The nature of the impurity or imperfection that produces the infrared absorption peaks, the semiconductivity, and the blue color of IIb diamonds is still uncertain, although boron is known to produce a blue coloration and semiconductivity in synthetic diamond (15).

In general, no direct correlation has been found between the observed optical and electrical properties of diamond and the amount or type of impurities known to be present (with the possible exception of nitrogen). Type IIa and IIb diamonds both contain Si, Mg, and Al in similar concentrations of approximately 10^{15} atoms per cc as the major impurities detected by spectrographic methods (19). Impurities commonly found in Type

I are Si, Ca, Mg, Al, Fe, Ti and Cu in concentrations as large as 10^{18}-10^{19} atoms per cc. Also, there is no apparent relationship between color and impurity content.

It is possible that the properties of semiconducting diamonds are due to lattice defects such as vacancies, interstitials, and dislocations. Imperfections in Type I and II diamonds have been found using the technique of transmission electron microscopy (20). The presence of nitrogen platelets on {100} planes and small dislocation loops on {111} planes near the platelets appeared in Type I diamonds but were not found in Type II diamond.

Electron Spin Resonance Studies in Diamond

The presence of nitrogen in diamond has been detected using electron spin resonance, which supports the results of optical studies (21). By this method it was found that nitrogen is a common paramagnetic impurity acting as a donor in diamond. Nitrogen enters the diamond lattice substitutionally with the donor electron occupying an antibonding orbital formed with a particular carbon nearest neighbor. Three equally spaced lines occur for the magnetic field parallel to the [001] direction. The symmetry axis for the hyperfine interaction with N^{14} was found to be along any one of the four nearest neighbor directions. Also, hyperfine interaction with C^{13} was detected. The g-value for the nitrogen donor was isotropic and equal to 2.0024. The line width between points of maximum slope was 0.3 gauss for most diamonds.

The lattice defects produced by neutron and electron irradiation give rise to paramagnetic resonance absorption. These centers have been studied by several investigators (22, 23, 24, 25). The observed spectra are

usually composed of a single isotropic line with more complex spectra superimposed. Explanation of the ESR spectra includes the interaction of vacancies with impurities, interstitials, single vacancies, and aggregates of defects.

Electron spin resonance has been detected in diamonds for various other defect centers, but the exact nature of the structure has remained uncertain (26, 27, 28).

CHAPTER II

ELECTRON SPIN RESONANCE

Classical Interpretation

Magnetic Resonance and Rotating Coordinates

In an electron spin resonance experiment the sample containing electron paramagnets is subject to a magnetic field $\vec{H}$ ($\vec{H}$ may be time dependent) and a microwave field $\vec{H}_1$ perpendicular to $\vec{H}$ and of constant frequency. To describe the motion of the electron spins $\vec{S}$ when placed in these fields the classical ideas of Bloch (30) concerning nuclear magnetic resonance are useful and according to which the nuclear paramagnets execute a Larmor precession in a magnetic field.

Initially the angular momentum of the electron is assumed to consist of the spin only component, although in the practical case one must consider the orbital contribution. The spin angular momentum $\hbar\vec{S}$ of the electron is associated with the magnetic moment $\vec{\mu}$ through the expression given previously

$$\vec{\mu} = -\gamma\hbar\vec{S}. \tag{2.1}$$

In the fixed laboratory system the z-axis of a rectangular coordinate system x, y, z is taken so that the magnetic field $\vec{H}$ is along the z-direction (Fig. 2-1a). According to classical electromagnetic theory a torque $\vec{T} = \vec{\mu} \times \vec{H}$ acts on the electron. This torque is also equal to the time rate of change of the electron angular momentum, $\hbar \frac{d\vec{S}}{dt}$, resulting in the following classical equation of motion in the fixed coordinate system:

$$\frac{d\vec{\mu}}{dt} = \gamma\vec{H} \times \vec{\mu}. \tag{2.2}$$

A solution to this equation can be obtained by transforming to a rotating coordinate system (31). The rotating system is shown in Fig. 2-1a where the z-axis, denoted by z_r, of the rotating coordinate system coincides with the z-axis of the fixed laboratory system. The axes x_r and y_r rotate about the common z-axis with an angular frequency $\vec{\omega}$. In the rotating system $\left(\frac{d\vec{\mu}}{dt}\right)_r$ denotes the time rate of change of $\vec{\mu}$ that an observer rotating with x_r would see, and $\vec{\omega} \times \vec{\mu}$ gives the rate of change due to the rotation of the axes. The equation of motion in terms of the rotating system is

$$\frac{d\vec{\mu}}{dt} = \left(\frac{d\vec{\mu}}{dt}\right)_r + (\vec{\omega} \times \vec{\mu}) \tag{2.3}$$

so that

$$\left(\frac{d\vec{\mu}}{dt}\right)_r = \left(\frac{d\vec{\mu}}{dt}\right) - (\vec{\omega} \times \vec{\mu}).$$

Using eq. (2.2) and rearranging gives

$$\left(\frac{d\vec{\mu}}{dt}\right)_r = \gamma\left(\vec{H} - \frac{\vec{\omega}}{\gamma}\right) \times \vec{\mu}. \tag{2.4}$$

This is the equation for $\vec{\mu}$ as seen from the rotating coordinate system. It is of the same form as the equation of motion in the stationary coordinate system with the difference being that $\vec{H}$ is replaced by the effective field

$$\vec{H}_e = \vec{H} - \frac{\vec{\omega}}{\gamma}. \tag{2.5}$$

If $\vec{H}$ is equal to a constant field H_o along the z-axis then H_e will disappear if $H_o = \frac{\omega}{\gamma}$, i.e., if

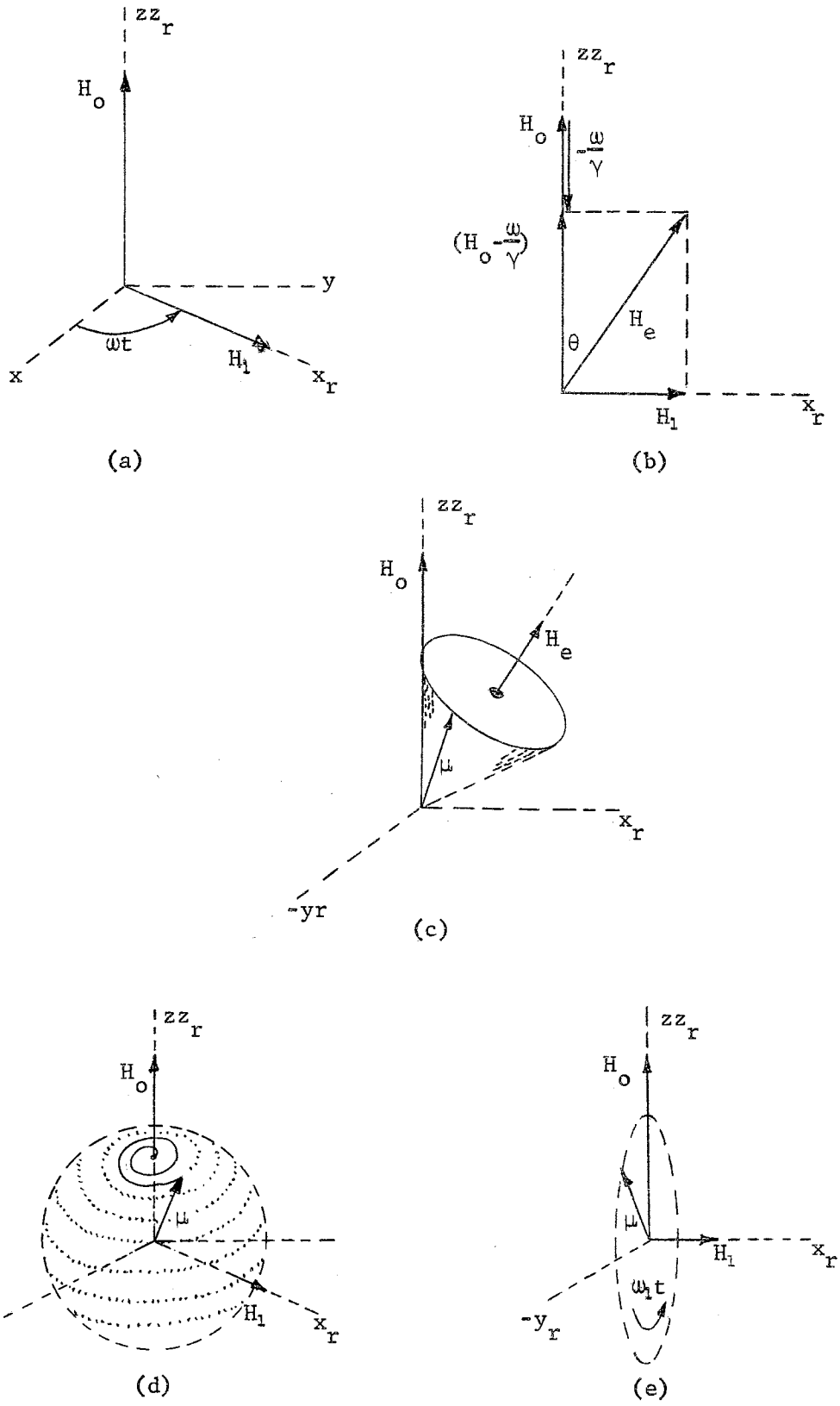

Figure 2-1. The rotating coordinate system and the motion of the magnetic moment $\vec{\mu}$ in the effective magnetic field $\vec{H}_e$.

$$\omega_o = \gamma H_o \tag{2.6}$$

Thus, $\left(\frac{d\vec{\mu}}{dt}\right)_r = 0$ and for an observer rotating about the z-axis with angular frequency ω_o given by eq. (2.6) the magnetic moment remains unchanged. In other words, the individual electron magnetic moments (hence, their spins) precess about the direction of the external magnetic field H_o with a frequency ω_o called the "Larmor frequency". Figure 2.2 shows the motion of $\vec{S}$ in the magnetic field $\vec{H}_o$. The change of $\vec{S}$ is perpendicular to both $\vec{S}$ and H_o with the angle θ remaining constant.

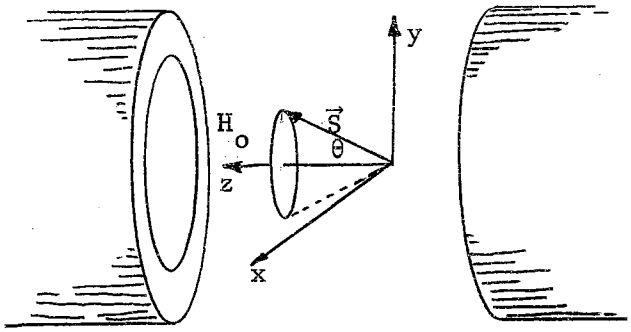

Figure 2-2. Precession of $\vec{S}$ in a magnetic field H_o.

The transformation just carried out is purely mathematical, and the precession of the individual electron spins could not be observed. In order to observe magnetic resonance an additional alternating magnetic field $\vec{H}_1$ must be introduced which is circularly polarized in the x-y plane and having components

$$H_x = H_1 \cos \omega t, \quad H_y = H_1 \sin \omega t. \tag{2.7}$$

The $\vec{H}_1$ field rotates about the z-axis with an angular frequency $\vec{\omega} = \omega\vec{k}$.

The magnetic field $\vec{H}$ is now no longer just a constant field H_o, but has an additional time-dependent field perpendicular to the field H_o. The total magnetic field is now represented in the fixed laboratory system by

$$\vec{H} = (H_1 \cos \omega t)\vec{i} + (H_1 \sin \omega t)\vec{j} + H_o\vec{k} \qquad (2.8)$$

where $\vec{i}$, $\vec{j}$, and $\vec{k}$ are the usual unit vectors along x, y, and z.

A transformation to the rotating coordinate system (r-system) may also be used to treat the case of the combined fields with the r-system rotating about the z-axis at the same angular frequency as $\vec{H}_1$. $\vec{H}_1$ is taken in the direction of the x_r-axis, see Fig. 2-1a. Equation (2.4) holds in the case where $\vec{H}$ is composed of two parts with the effective field

$$\vec{H}_e = H_1 \vec{i}_r + (H_o - \frac{\omega}{\gamma}) \vec{k}_r. \qquad (2.9)$$

The physical situation corresponding to eq. (2.9) is shown in Fig. 2-1c. The effective field $\vec{H}_e$, as viewed from the r-system, acts as a constant magnetic field and the magnetic moment initially in the z-direction will precess in a cone about $\vec{H}_e$ at an angular frequency $\omega_e = \gamma H_e$.

The same results could have been arrived at by introducing a second rotating coordinate system (rr-system) and requiring that $\left(\frac{d\vec{\mu}}{dt}\right)_{rr} = 0$, which means that $\vec{\mu}$ would remain unchanged in the doubly rotating system. The complete motion of $\vec{\mu}$ when observed from the laboratory system is the precession about $\vec{H}_e$ plus the rotation of the x_r-axis about the constant field H_o. Such a motion of the magnetic moment vector under the influence of both $\vec{H}_1$ and H_o is shown in Fig. 2-1d.

In order to gain some insight into the motion of $\vec{\mu}$ under the influence of $\vec{H}$, now a time-dependent field, consider the situation when $\omega = \gamma H_o$ and the motion is observed from the rotating system. The magnetic field components in the r-system are shown in Fig. 2-1b where the angle θ is given by

$$\cos\theta = \frac{H_o - \frac{\omega}{\gamma}}{H_e}, \quad \sin\theta = \frac{H_1}{H_e} \tag{2.10}$$

and the magnitude of the effective field is

$$H_e = \left[\left(H_o - \frac{\omega}{\gamma}\right)^2 + H_1^2\right]^{\frac{1}{2}} \tag{2.11}$$

When $\omega = \gamma H_o$ we would expect, on the basis of the preceding discussion, a precession of $\vec{\mu}$ about the x_r-axis ($\vec{H}_e$ direction) with an angular frequency $\omega_1 = \gamma H_1$. From consideration of the rr-system and r-system one can arrive at the following expressions for the components of the magnetic moment, in the r-system, with $\omega = \gamma H_o$ and $H_e = H_1$:

$$\begin{aligned} \mu_{x_r} &= 0 \\ \mu_{y_r} &= -\mu \sin \omega_1 t \\ \mu_{z_r} &= \mu \cos \omega_1 t \end{aligned} \tag{2.12}$$

Therefore, in the r-system the magnetic moment vector precesses in a plane perpendicular to the effective field and periodically changes its orientation along the z-axis at a frequency $\omega_1 = \gamma H_1$ (see Fig. 2-1e). The complete reorientation of the magnetic moment $\vec{\mu}$ in the magnetic field H_o when $\omega_o = \gamma H_o$ is the magnetic resonance phenomena. One thing to note is that the magnetic moment $\vec{\mu}$ executes many more Larmor precessions in the field H_o compared to the number in the field H_1 ($\omega_1 \ll \omega_o$), i.e., a slow tipping of the vector $\vec{\mu}$ occurs as it precesses rapidly around H_o.

Phenomenological Description of Magnetic Resonance with Relaxation Effects

For the case of interacting spins the relaxation times and equations of motion obtained by Bloch for nuclear spins are applicable. Bloch (30) assumed the following form to describe the magnitude of the "longitudinal

magnetization" at time t ($\vec{M} = \Sigma \vec{\mu}$)

$$M_z = M_o \left[1 - \exp\left(-\frac{t}{T_1}\right)\right] \tag{2.13}$$

where $M_o = \chi_o H_o$ is the equilibrium magnetization at temperature T; χ_o is the static magnetic susceptibility and H_o the static magnetic field. T_1 is generally referred to as the "spin-lattice relaxation time". The rate of change of M_z is then given by

$$\dot{M}_z = \frac{dM_z}{dt} = \frac{M_o - M_z}{T_1} . \tag{2.14}$$

As a result of the application of the rotating magnetic field H_1 a second relaxation time T_2 is introduced describing the decay of the transverse magnetization. The relaxation time T_2 involves the process of energy exchange within the spin system and is called the "spin-spin relaxation time". The components of the transverse magnetization M_x and M_y decay in the following manner:

$$\dot{M}_x = -\frac{M_x}{T_2} , \quad \dot{M}_y = -\frac{M_y}{T_2} . \tag{2.15}$$

The equation of motion in the absence of relaxation effects

$$\frac{d\vec{M}}{dt} = \gamma \vec{H} \times \vec{M} \tag{2.2}$$

becomes for the interacting electrons with $H_1 \ll H_o$

$$\frac{d\vec{M}}{dt} = \gamma \vec{H} \times \vec{M} - \frac{M_x \vec{i} + M_y \vec{j}}{T_2} - \frac{M_z - M_o}{T_1} \vec{k} \tag{2.16}$$

Since $\vec{H} = (H_1 \cos \omega t)\, \vec{i} + (H_1 \sin \omega t)\, \vec{j} + H_o \vec{k}$ the components M_x, M_y and M_z change with time according to the equations

$$\dot{M}_x = \gamma(M_z H_1 \sin \omega t - M_y H_o) - \frac{M_x}{T_2} \tag{a}$$

$$\dot{M}_y = \gamma(H_o M_x - M_z H_1 \cos \omega t) - \frac{M_y}{T_2} \qquad (b) \quad (2.17)$$

$$\dot{M}_z = \gamma(M_y H_1 \cos \omega t - M_x H_1 \sin \omega t) + \frac{M_o - M_z}{T_1} \qquad (c)$$

In the rotating coordinate system the components of the transverse magnetization M_u and M_v are related to M_x and M_y by

$$\begin{aligned} M_u &= M_x \cos \omega t + M_y \sin \omega t \\ M_v &= M_y \cos \omega t - M_x \sin \omega t \end{aligned} \qquad (2.18)$$

solving for M_x and M_y

$$\begin{aligned} M_x &= M_u \cos \omega t - M_v \sin \omega t \\ M_y &= M_u \sin \omega t + M_v \cos \omega t \end{aligned} \qquad (2.19)$$

Equations (2.17 a,b,c) transformed to the rotating system using (2.18) and (2.19) are as follows:

$$\dot{M}_u + (\omega_o - \omega) M_v = -\frac{M_u}{T_2} \qquad (a)$$

$$-\dot{M}_u + (\omega_o - \omega) M_u - \omega_1 M_z = \frac{M_v}{T_2} \qquad (b) \quad (2.20)$$

$$\dot{M}_z - \omega_1 M_v = \frac{M_o - M_z}{T_1} \qquad (c)$$

where $\omega_o = |\gamma| H_o$ and $\omega_1 = |\gamma| H_1$. The solutions to these equations are obtained by using an approximation utilizing slow passage through the resonance line. The condition of slow passage relates the scanning rate of the magnetic field H_o, $\frac{dH_o}{dt}$, to the relaxation times. Specifically, the time of passage through the resonance line must be long compared to the relaxation times so that the magnetization can be considered to have its

equilibrium value. Therefore, the condition $\dot{M}_x = \dot{M}_y = \dot{M}_z = 0$ is consistent with the slow passage requirement. Under this condition the algebraic relations between equations (2.20) give the three components of the magnetization in the rotating coordinate system:

$$M_u = \frac{M_o \omega_1 T_2^2 (\omega_o - \omega)}{[1 + \omega_1^2 T_1 T_2 + T_2^2 (\omega_o - \omega)^2]} \qquad (a)$$

$$M_v = - \frac{M_o \omega_1 T_2}{[1 + \omega_1^2 T_1 T_2 + T_2^2 (\omega_o - \omega)^2} \qquad (b) \quad (2.21)$$

$$M_z = \frac{M_o [1 + T_2^2 (\omega_o - \omega)^2]}{[1 + \omega_1^2 T_1 T_2 + T_2^2 (\omega_o - \omega)^2]} \qquad (c)$$

Assuming a weak alternating field $\vec{H}_1$ ($\omega_1^2 T_1 T_2 \ll 1$) the equations (2.21a) and (2.21b) can be graphed yielding M_u and M_v as functions of $T_2 (\omega_o - \omega)$. Such a plot, as indicated in Fig. 2-3a, shows that the curves are representative of the dispersive and absorptive modes of a harmonic oscillator. The end point of the transverse magnetization vector M_t is found to move

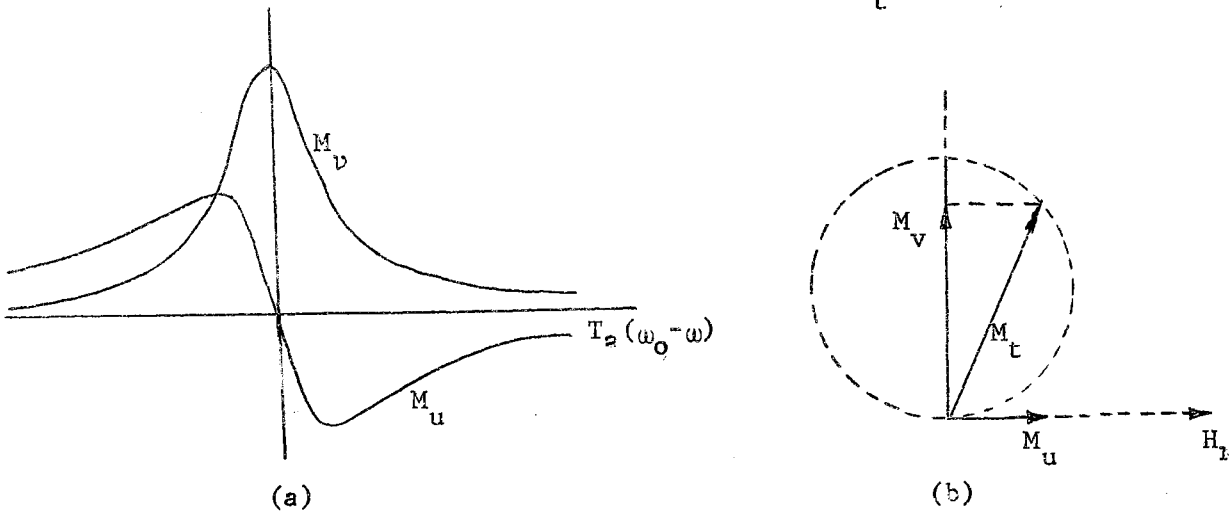

Figure 2-3. Transverse magnetization; (a) dispersive and absorptive modes, (b) vector relationship in rotating frame.

in a circle as shown in Fig. 2-3b. It should be noted that at resonance the transverse magnetization is shifted in phase with respect to $\vec{H}_1$ by 90^o and equal to the maximum value of M_v.

If the high frequency susceptibility $\chi = \chi' - i\chi''$ is introduced and M_x is taken to be the real part of the complex quantity $\chi\,[2H_1 \exp(i\omega t)]$

$$M_x = \chi' 2H_1 \cos \omega t + \chi'' 2H_1 \sin \omega t \tag{2.22}$$

Comparing this equation with equation (2.16) shows that

$$\chi' = \frac{M_u}{2H_1}\,, \quad \chi'' = -\frac{M_v}{2H_1} \tag{2.23}$$

where χ' gives the dispersion curve and χ'' is responsible for the absorption of energy from the high frequency field. The power absorbed by the spin system is given by

$$P = 2\omega H_1^2 \chi''$$

so that

$$\begin{aligned} P &= \chi_o \omega T_2 \frac{\omega_o H_1^2}{[1 + T_2^2(\omega_o - \omega)^2]} \\ &= \pi \chi_o \omega \omega_o H_1^2 \, L(\omega) \end{aligned} \tag{2.24}$$

where

$$L(\omega) = \frac{T_2}{\pi} \frac{1}{1 + T_2^2(\omega_o - \omega)^2}$$

is the Lorentzian line shape function. The width of the resonance line at half intensity, $\Delta\omega = 2(\omega_o - \omega)$, is given by

$$\Delta\omega = \frac{2}{T_2}$$

or written in magnetic field units

$$\Delta H = \frac{2}{\gamma T_2} \tag{2.25}$$

To obtain the resonance line experimentally the magnetic field is slowly varied as the high frequency field is held constant. A more detailed account of the Bloch method can be found in the book by Abragam (32).

Remarks on the Observation of Electron Spin Resonance

The value of the applied magnetic field H_o determines the frequency at which ESR will be observed. A desirable frequency occurs in the microwave region; and, therefore, the sample is usually placed in a microwave cavity. The ESR effect produces an increase in the resistive losses of the cavity and, in addition, changes the characteristic reactance of the cavity. The out-of-phase component of the susceptibility, χ'', is responsible for the absorption of microwave energy with the dispersion given by the in-phase component χ'. The ESR apparatus must be capable of measuring and recording χ'' and χ'. Once the signal is obtained the theoretical expression for this signal is the solution to Bloch's equations.

CHAPTER III

ELECTRON SPIN RESONANCE INSTRUMENTATION

Electron Spin Resonance Spectrometer

General Description of ESR Spectrometers

The instruments used in ESR spectrometers perform the same basic functions as those used for nuclear magnetic resonance, although microwave techniques are generally used for electron spin resonance in contrast to the radiofrequency circuits of nuclear resonance. The frequency region for ESR arises from the fact that the gyromagnetic ratio of the electron is approximately 2.80 megacycles per gauss compared to 4.26 kilocycles per gauss for proton resonance. Although the operating frequency for a particular experimental situation may be optimized (with regard to sample size, saturation, available magnet, etc.), the most common ESR spectrometers operate in the x-band region of the microwave spectrum near 9.5 kMc. This requires a magnetic field of approximately 3400 gauss for the free electron resonance.

Basically, there are two common types of electron spin resonance spectrometers; one form utilizes the reflection cavity, the other a transmission cavity. The reflection cavity is the most versatile and is used extensively in the usual bridge spectrometer. To detect ESR signals the sample is placed in a reflection cavity in the magnetic field of an electromagnet with incident microwave energy. Since it is inconvenient to vary

the microwave frequency the magnetic field is scanned so that the resonance condition, $h\nu = g\beta H$, is satisfied. The field configuration of the cavity is selected so that the microwave magnetic field is perpendicular to the applied polarizing field H. If the resonance condition is satisfied then energy is absorbed from the microwave field and the additional instrumentation associated with ESR spectrometers must detect this absorption.

The basic electron spin resonance spectrometer usually consists of the following components (see Figure 3-1):

(1) An electromagnet providing a sufficiently homogeneous magnetic field, with its associated power supply, and a method by which the field can be linearly swept through the resonance line.

(2) A source of microwave energy, usually a reflex klystron, that is frequency stabilized and has a power output near 100 milliwatts.

(3) A magnetic field modulation system that introduces a small alternating component to the linear sweep of the constant magnetic field. This modulating field is added to the constant field by the use of modulation coils mounted on the cavity, dewar system, or magnet pole pieces. Also, the modulation oscillator provides a reference voltage for the phase-sensitive detector used in a narrow-band detection system.

(4) A microwave circuit that allows microwave energy to be introduced into the cavity and permits the monitoring of the reflected energy from the cavity. The usual circuit configuration includes a magic "T" as the bridge element, but other forms are possible that use a directional coupler or a microwave ferrite circulator. The microwave detection system can incorporate either crystal diodes or bolometers (barretters) in the circuit.

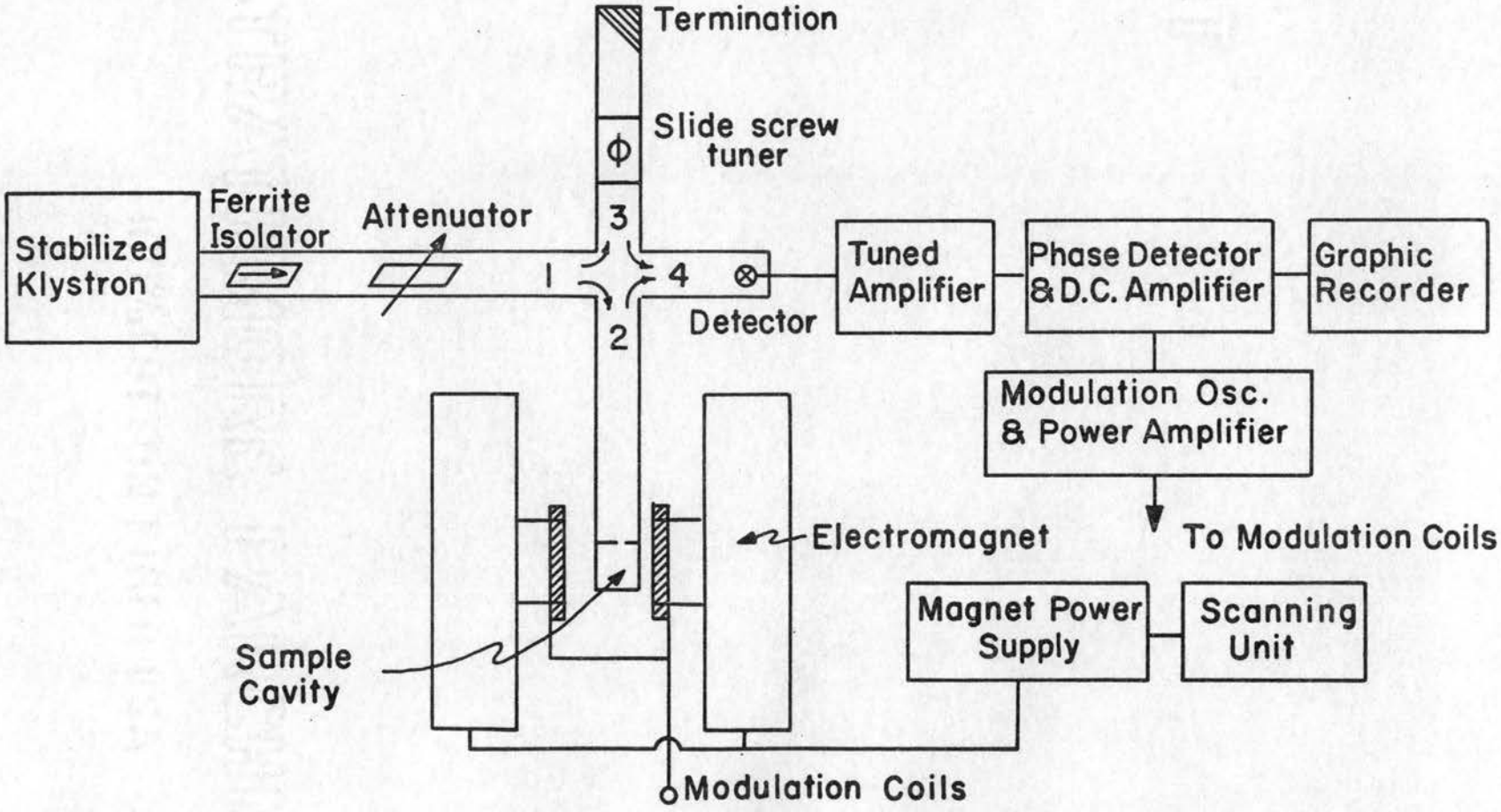

Fig. 3-1 Basic Components of an ESR Bridge Spectrometer

(5) An ESR signal amplifier and a phase-sensitive detector operating at the frequency of the magnetic field modulation. The output of the phase detector is recorded graphically by using a pen recorder or an oscilloscope.

(6) A sample cavity in which the sample is placed. It is imperative that the Q and the coupling of the cavity to the waveguide be optimized so as to obtain maximum detectibility from the instrument.

Description of the ESR Spectrometer Used in This Investigation

Magnet System

An x-band ESR spectrometer operating at 9.5 kMc requires (for g = 2) a magnetic field of 3400 gauss with a homogeneity of slightly better than 0.1 gauss over a minimum volume of 1 cm^3 (3). These requirements are based on ESR work in solids where line widths are not as narrow as those found in liquids or in nuclear resonance and are usually not less than 100 milligauss. Since the magnet system is probably the most expensive single system in the ESR spectrometer, it must be chosen partly from the economic view; however, when possible a magnet of sufficient homogeneity for very narrow lines should be obtained. The magnetic field must be swept over a large range and the magnet power supply, in addition to being highly regulated, should have a provision for sweeping the magnetic field. Other factors in the selection of a magnet includes consideration of the gap geometry so as to allow for various cavity shapes and for cryogenic equipment.

Initially the magnet system consisted of a Varian 4" magnet and a battery power supply. Batteries are inconvenient to use since the voltage decreases with time and the magnet resistance changes because of temperature fluctuations; therefore, an electronic regulation system was considered necessary. In such a current regulating system the usual procedure

is to monitor and compare the voltage generated across a standard resistor e_o with a reference voltage e_{ref} (see Fig. 3-2).

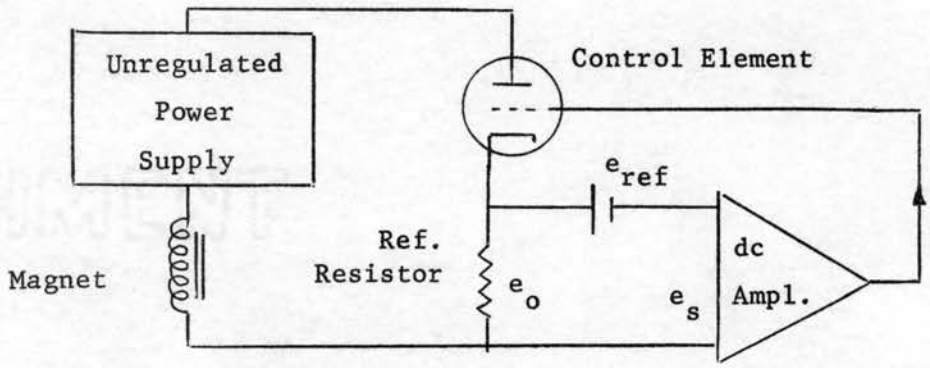

Figure 3-2. Regulation of the magnet current.

Any difference in the voltages e_o and e_{ref}, designated e_s (dc error voltage), is amplified and fed back to the magnet current control element in such a way as to make $e_s = 0$. The control element becomes a variable series resistance controlled by the amplified error signal. Such a control element is shown in Figure 3-2 as a vacuum tube, but power transistors can also be used when appropriate. In fact, vacuum tube control elements require highly regulated voltages and the system can become quite complex and inefficient.

The Varian 4" magnet coils can be connected in a parallel arrangement yielding a fairly low impedance system and the use of power transistors was considered as the control element for the magnet current. Articles describing transistor current regulators for magnets have been published (33, 34, 35). Use was made of the transistor regulator described by Garwin (35), although for an integrated compact system the design of Johnson and Singer (34) has desirable characteristics. The articles adequately describe the circuit used and only a few comments of practical importance will be mentioned. First, the control of the main power to the magnet

TABLE I

OPERATION OF VARIAN 4" MAGNET USING
A TRANSISTOR CURRENT REGULATOR

A. Turn on Procedure

1. Set Variac to approximately 10-15 volts input to magnet. Magnet switch is in off position until indicated below.

2. Turn on: (a) Null Indicator, set at full gain

   (b) Water to power transistors, magnet, and reference resistor

   (c) Transistor amplifier

   (d) Reference voltage and sweep control.

3. Adjust reference voltage by using coarse adjustment to 0.20.

4. Turn on switch to supply power to the magnet.

5. Monitor collector-emitter voltage on power transistors and maintain at least 6-10 volts bias.

6. Increase Variac, but do not exceed 25 volts on power transistors for 2 amps. current. In fact, do not exceed 25 volts under any circumstances to be safe. Initially set the collector-emitter voltage at 10 volts; then increase the Variac in steps of about 15 volts until desired current is reached.

B. Turn off Procedure

1. Reduce magnet current by adjusting reference voltage. On reaching collector-emitter voltage of 25 volts reduce Variac by 15 volts until magnet current is minimum.

2. Open Magnet switch.

3. Turn off: (a) Transistor amplifier.

   (b) Null Indicator

   (c) Water

   (d) Reference and sweep voltages.

should be convenient for manual control with a form of automatic (servo system) control incorporated into the system to hold the power transistors below their rated power dissipation when initial adjustments are made or when large sweeping currents are required. Servo controlled Variacs are now available and would be useful in this respect. A set of operating instructions is given in Table I for the control system used. Table I is given merely as a guide for the particular system that was used. The main power to the magnet was controlled from a panel located in an adjacent room, hence, the reason for such an operating procedure. Second, a variable voltage for sweeping the magnetic field can be placed into the system at the junction between the reference resistor and the reference voltage source; this sweep voltage should be variable from (+) to (-). The operation of the system seemed adequate after a reasonable warm-up time. Further refinements or changes in the circuit were not undertaken since a Varian 6" rotating magnet with ring shim pole pieces was purchased with its own regulated power supply.

The Varian 6" rotating magnet, Model 4007-1, can be turned about its vertical axis (a full 200^{o} on the pedestal base) to allow single crystal orientation studies to be performed without disturbing the sample in the microwave cavity. Two problems arise on rotating the magnetic field: (a) the microwave magnetic field must always remain perpendicular to the magnetic field, and (b) the modulation field must remain in the direction of the magnetic field. A more complete discussion of these problems will be included in the section on microwave cavities and in connection with the modulation system.

The magnetic field contour is shown in Fig. 3-3 for the Varian 6" magnet with ring shim pole pieces. A gap of 2.875" accommodates the double

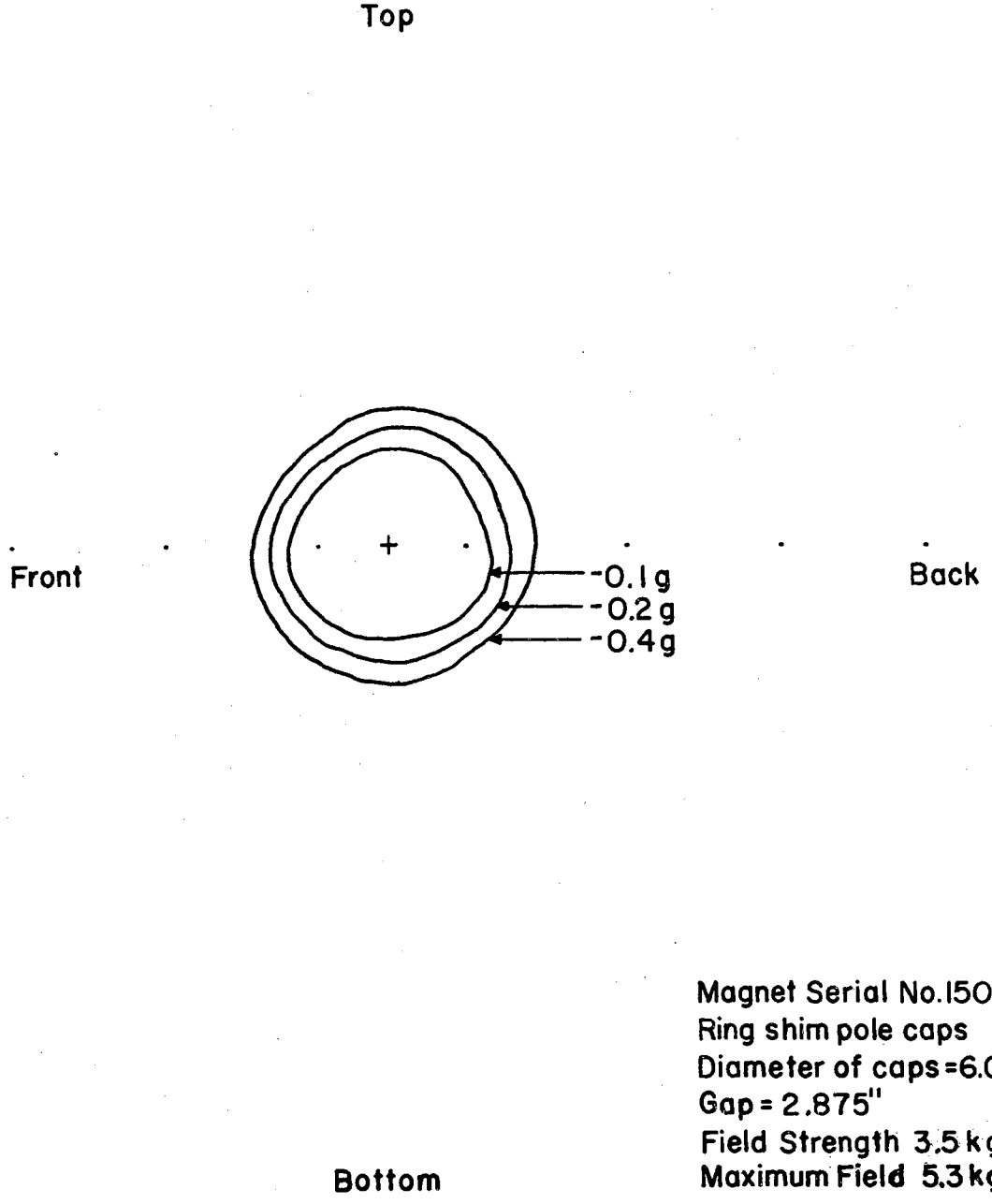

Fig. 3.3 Magnetic Field Plot of Varian Model V4007-1 Electromagnet

dewar liquid helium system manufactured by Varian Associates.

Klystron Frequency Stabilization

In a sensitive ESR spectrometer it is necessary to stabilize the frequency of the klystron over the period of time required to record the spectra. Stabilization not only increases the signal-to-noise ratio, but prevents the admixture of the real χ' and imaginary χ'' parts of the susceptibility with a simplification of the recorded data. The stabilization system proven to be satisfactory for resonance work is the Pound i.f. circuit (36, 37) or its modified form (38, 39). The modified or "equal arm" microwave discriminator is shown in Fig. 3-4. The circuit utilizes a magic-T with the reference cavity and the modulating crystal in the comparison arms of the "T". Microwave power from the klystron is coupled to the discriminator through the 20 db directional coupler into arm 1 (H arm). The carrier frequency entering arm 3 is modulated at 30 mc, and the two generated sidebands return to the junction on reflection. Part of this modulated wave returns to arm 1 and is dissipated while the wave entering arm 4 (E arm) is mixed with the wave reflected from the reference cavity. Any difference in the frequency of the klystron and the resonance frequency of the reference cavity will introduce a reactive component into the reflected wave from the cavity. The phase of the reflected wave differs by 180° on either side of the resonance frequency. At the detector crystal the unmodulated wave reflected from the cavity mixes with the 30 mc modulated wave to give a 30 mc signal with an amplitude proportional to the frequency deviation of the klystron and a phase that differs by 180° on either side of the cavity resonance. The error signal is then amplified in a 30 mc i.f. amplifier and compared with a reference signal from the

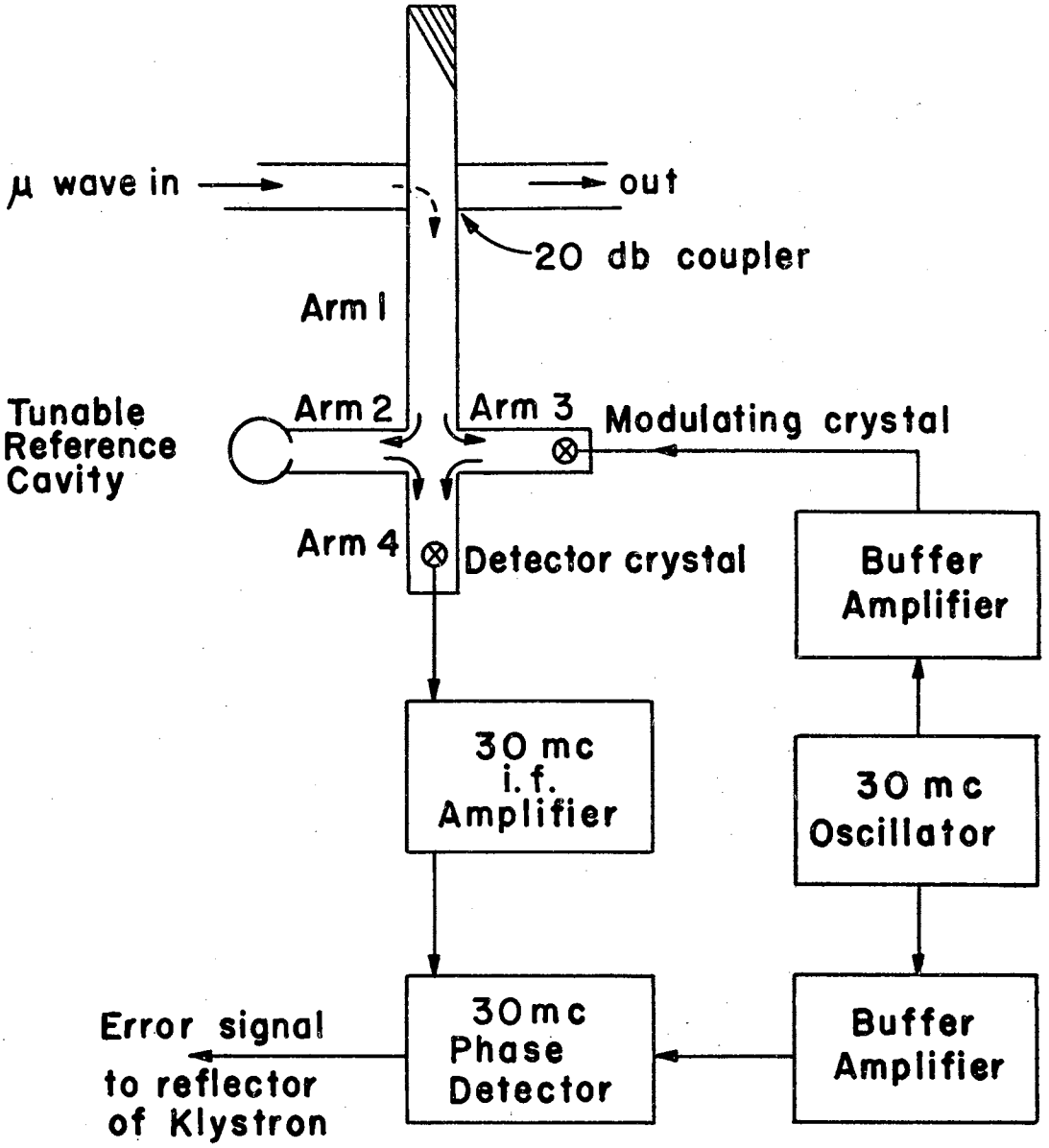

FIG.3-4 Modified Pound Frequency Stabilizer

30 mc oscillator in a crystal diode phase detector. The output of the phase detector is a ± dc voltage with a magnitude determined by the frequency deviation and the sign depending on the phase of the 30 mc signal. The dc error signal is amplified and applied to the reflector of the klystron in such a manner as to correct for the frequency deviation and locks the klystron frequency to that of the reference cavity. This method of stabilization requires the isolation of the phase detector circuit from ground since the klystron reflector is at a high negative potential. A 30 mc phase detector using crystal diodes was constructed and is shown in Fig. 3-5. The output of the phase detector is amplified by a transistor dc differential amplifier and then applied to the klystron reflector. Figure 3-6 shows the circuit of the dc amplifier that was designed for use in the klystron stabilizer. The transistor amplifier is mounted directly on the back of the microammeter.

In addition to the electronic frequency stabilization, the klystron is thermally protected by immersion in a silicone oil bath that is water cooled. All microwave components are mounted on a vibration free support to reduce the effects of microphonics. Also, since power reflected back to the klystron affects its frequency, there should be a device to isolate the klystron from its load. Such isolation devices take the form of simple resistive attenuators or, better still, a ferrite isolator that passes energy in the forward direction with no attenuation but reduces any reflected energy. A ferrite isolator is used in this ESR spectrometer.

The power supplied to the electrodes of the klystron is well regulated using a commercial power supply, and the klystron filament current is supplied by the transistorized dc supply of Fig. 3-7. All these precautions tend to reduce the noise in the spectrometer system and provide better

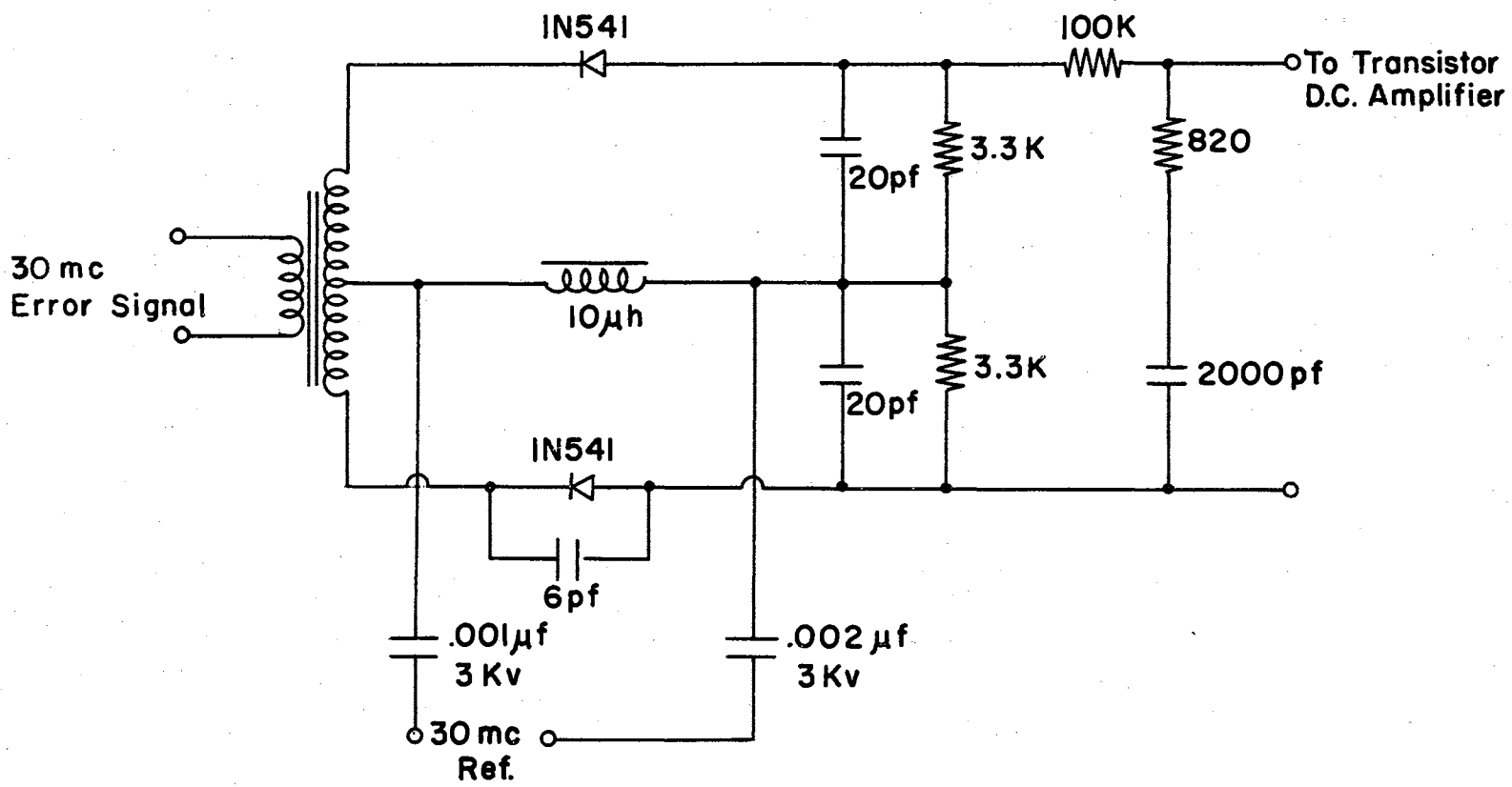

Fig. 3–5 30 mc Phase Detector

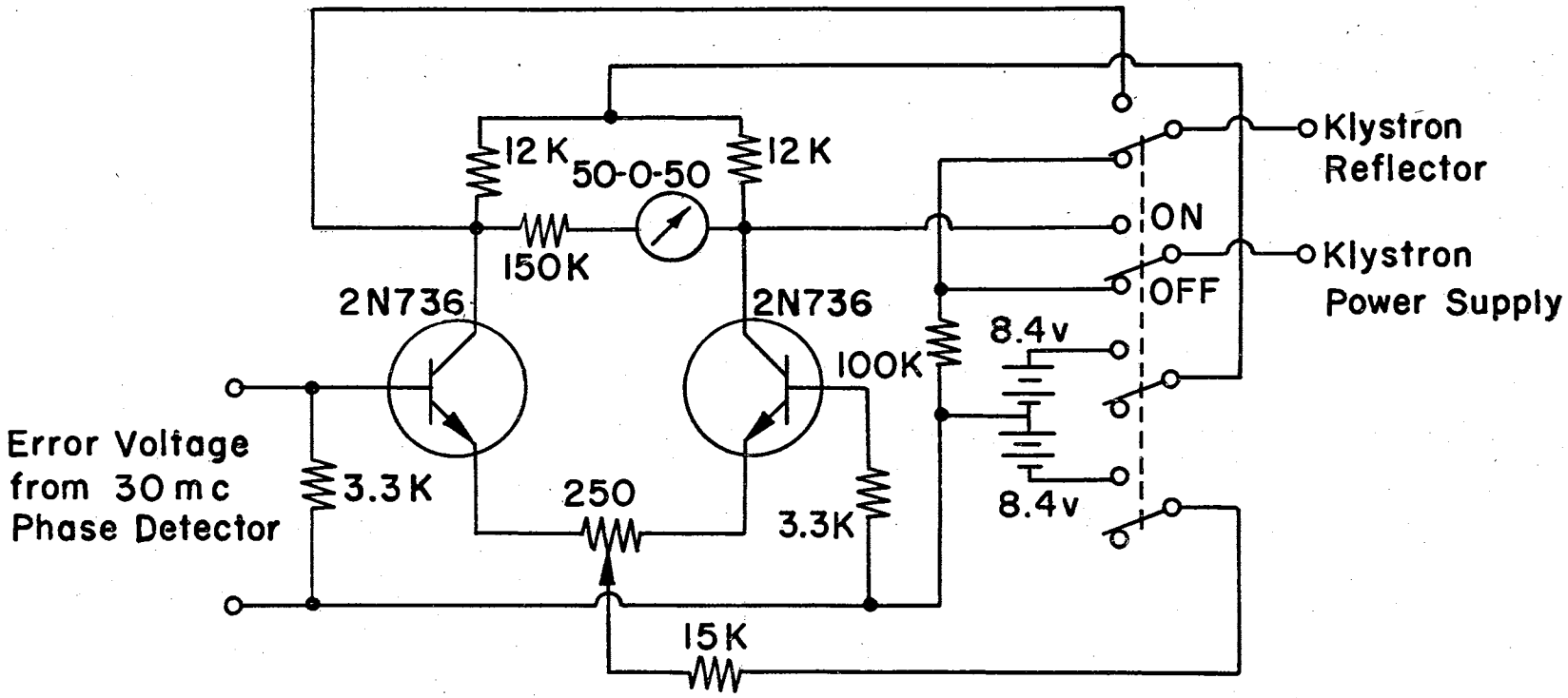

Fig. 3–6 Transistor Differential Amplifier

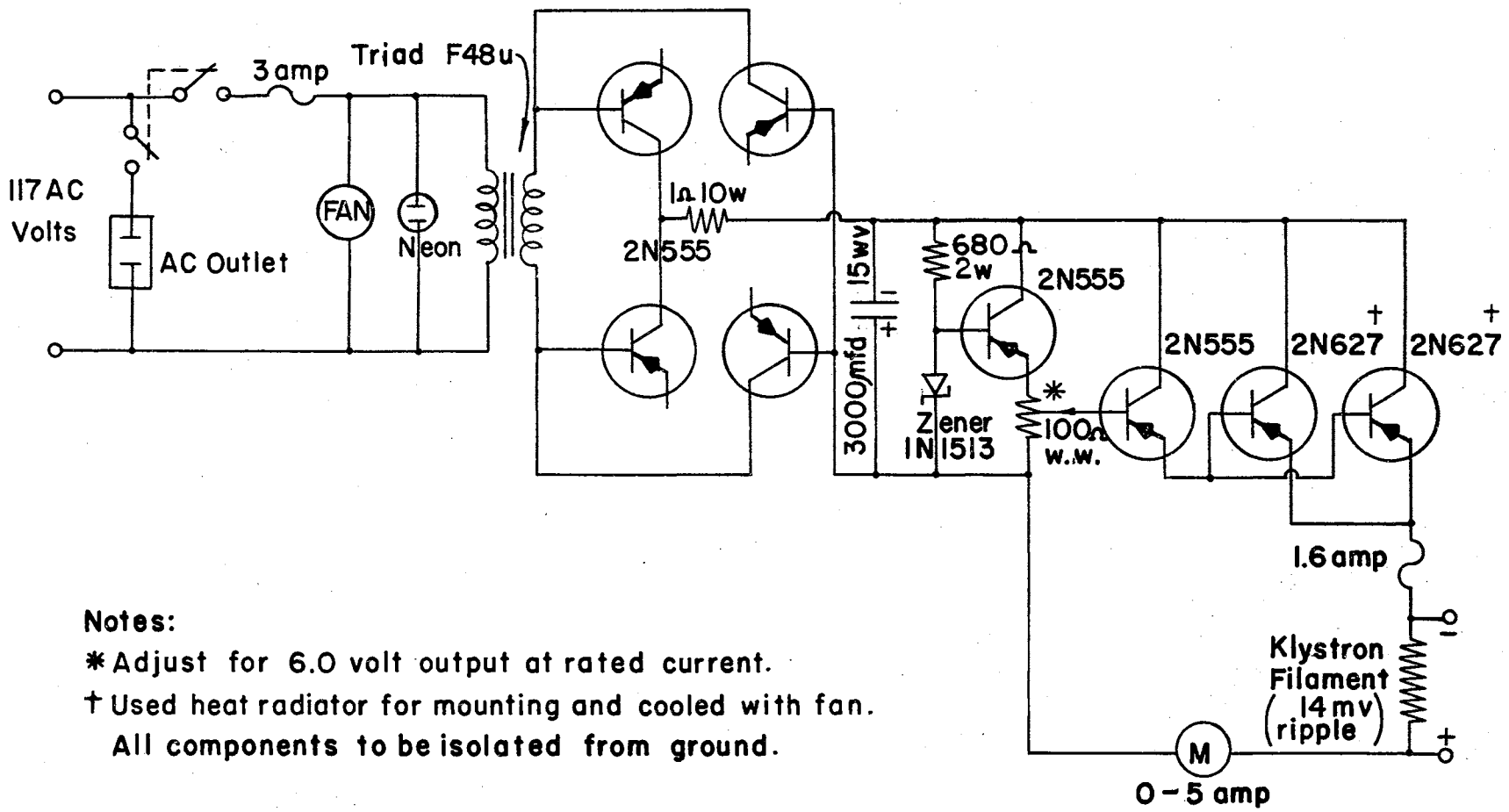

Notes:

* Adjust for 6.0 volt output at rated current.

† Used heat radiator for mounting and cooled with fan.
All components to be isolated from ground.

FIG. 3-7 Klystron Filament Supply

over-all performance.

Magnetic Field Modulation

In order to avoid the inherent instability of dc signal amplifiers the magnetic field is usually modulated as it is swept through resonance so that ac methods may be used. The modulation of the magnetic field can be accomplished by mounting coils on the sides of the sample cavity, the magnet pole pieces, the dewar system, or rigidly supporting loops inside the cavity when high frequency modulation is needed. The line width and shape of ESR lines vary considerably, and it is necessary for maximum sensitivity to include an amplitude control for the modulation so that very small (approximately 0.01 gauss) as well as large (over 10 gauss) modulating fields are available.

If a crystal rectifier is used to detect the ESR signal, then the crystal noise limits the available sensitivity depending on the modulation frequency. The noise power of a crystal rectifier varies as $\Delta f/f$, where Δf is the bandwidth at the modulation frequency f. Therefore, the noise voltage is inversely proportional to $\sqrt{f}$ and is shown graphically in Fig. 3-8. This means at some low frequency,

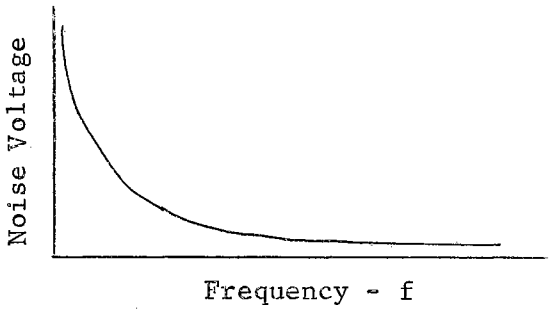

Figure 3-8. Characteristic noise spectrum of crystal diode detector.

for instance 100 cps, the noise voltage is $(f/100)^{\frac{1}{2}}$ times that at f. At f = 100 kc the noise voltage is approximately 1/30 that at 100 cps for the same bandwidth Δf. Thus, the signal-to-noise ratio can be improved by a factor of 30 considering only this source of noise. Another advantage in high modulation frequencies is that it permits, for the same signal-to-noise ratio, an increase in the bandwidth by almost 1000 in the above case. This allows, through the reduction of the time constant of the circuit (1/1000), an increase in the scanning rate assuming no other factors are involved. Bolometer detectors do not have the f^{-1} dependence of the noise and may be used advantageously at low frequencies.

One of the difficulties which restricts the use of extremely high modulation frequencies is the need to obtain fairly large modulation amplitudes at the sample location within the cavity. The cavity walls attenuate the high frequency fields considerably, and at 100 kc the wall must be metallic plated glass or ceramic, or the modulating coils must be placed on the inside of the cavity. Also, the modulation frequency must be kept small with respect to the line width (in frequency units) because the process of modulation broadens the absorption line with the broadening being proportional to the modulation frequency (41). It should be noted that eddy currents induced in the microwave cavity wall interact with the large magnetic field. The forces on the walls produced by the interaction cause wall vibrations that are proportional to the magnetic field and results in a synchronous periodic change in the cavity frequency at the modulation frequency. This signal is passed through the detection system as unwanted noise.

The high frequency modulation system used in this investigation is a Varian 100 kc control unit consisting of a tuned amplifier, phase detector,

100 kc crystal oscillator, and a modulation amplifier to drive the modulation coils on the sides of a ceramic cavity. The Varian 100 kc cavity will accommodate a variable temperature apparatus but has the disadvantage that the magnetic field can not be rotated when using this system.

The low frequency modulation system has several interesting features. First, bolometers are used to detect the ESR signal which can be modulated at 28, 400, and 1000 cps. Second, a low-noise transistor amplifier is used in conjunction with the bolometer bridge circuit. Third, the phase-sensitive detector utilizes a low noise Bristol synchroverter capable of being driven at any frequency from zero to approximately 1800 cps. Thus, the synchroverter can be used over the useful range of the low frequency response of the bolometers.

Microwave Circuit

A basic ESR spectrometer using a reflection cavity and microwave bridge circuit is illustrated in Fig. 3-1. The four-arm junction is the so-called magic-T structure that forms the basis for the bridge circuit at microwave frequencies. The theory of such bridge circuits is well described in the literature (36), and only a brief description will be given here in connection with its function in the ESR spectrometer. Power that is introduced into arm 1 is divided equally between the arms 2 and 3 if these arms are terminated with matched loads. No power reaches arm 4 as long as arms 2 and 3 remain matched. In practice, arm 2 is terminated with the sample cavity, and a slide screw tuner followed by a matched load is placed in arm 3. In the absence of a resonance signal the bridge is balanced, and no signal reaches the detector in arm 4. However, when the resonance condition is satisfied and the sample in the cavity absorbs energy from the

system, then the bridge becomes unbalanced with a resultant energy flow into arm 4. It should be pointed out that the condition of complete bridge balance is not the condition of optimum sensitivity and a small unbalance is usually introduced. Thus, the slide screw tuner is adjusted to introduce into arm 4 the desired amount of power. Another very important reason for having a slight amount of unbalance is that either the dispersive χ' or absorptive χ'' component of the magnetic susceptibility may be selected by proper adjustment of the bridge which simplifies data analysis.

The electron spin resonance spectrometer constructed and used in the initial investigations was a conventional x-band microwave bridge. Later modifications of the bridge spectrometer included the use of a ferrite circulator (42) and the inclusion of a balanced bolometer detection system (43). Figure 3-9 shows the block diagram of the various components comprising the bridge spectrometer. The x-band microwave energy is obtained from a Varian klystron, VA-201B or V-262, which has voltages supplied by a well-regulated power supply. The frequency of the klystron is stabilzed by coupling a small amount of microwave power into the modified Pound stabilizing circuit utilizing a high-Q invar cavity as the reference element. The klystron and klystron frequency stabilizing system are isolated from the rest of the bridge circuit by using a unidirectional ferrite isolator. The microwave frequency can be measured accurately with a Hewlett-Packard transfer oscillator and electronic counter. The electronic counter is also used to monitor the frequency of the nuclear resonance signal for magnetic field measurements. An adjustable precision attenuator permits the microwave power incident upon the sample bridge to be varied. The bridge itself is comprised of a matched magic-T with the reference arm consisting of a slide screw tuner and matched load. The arm containing the sample cavity

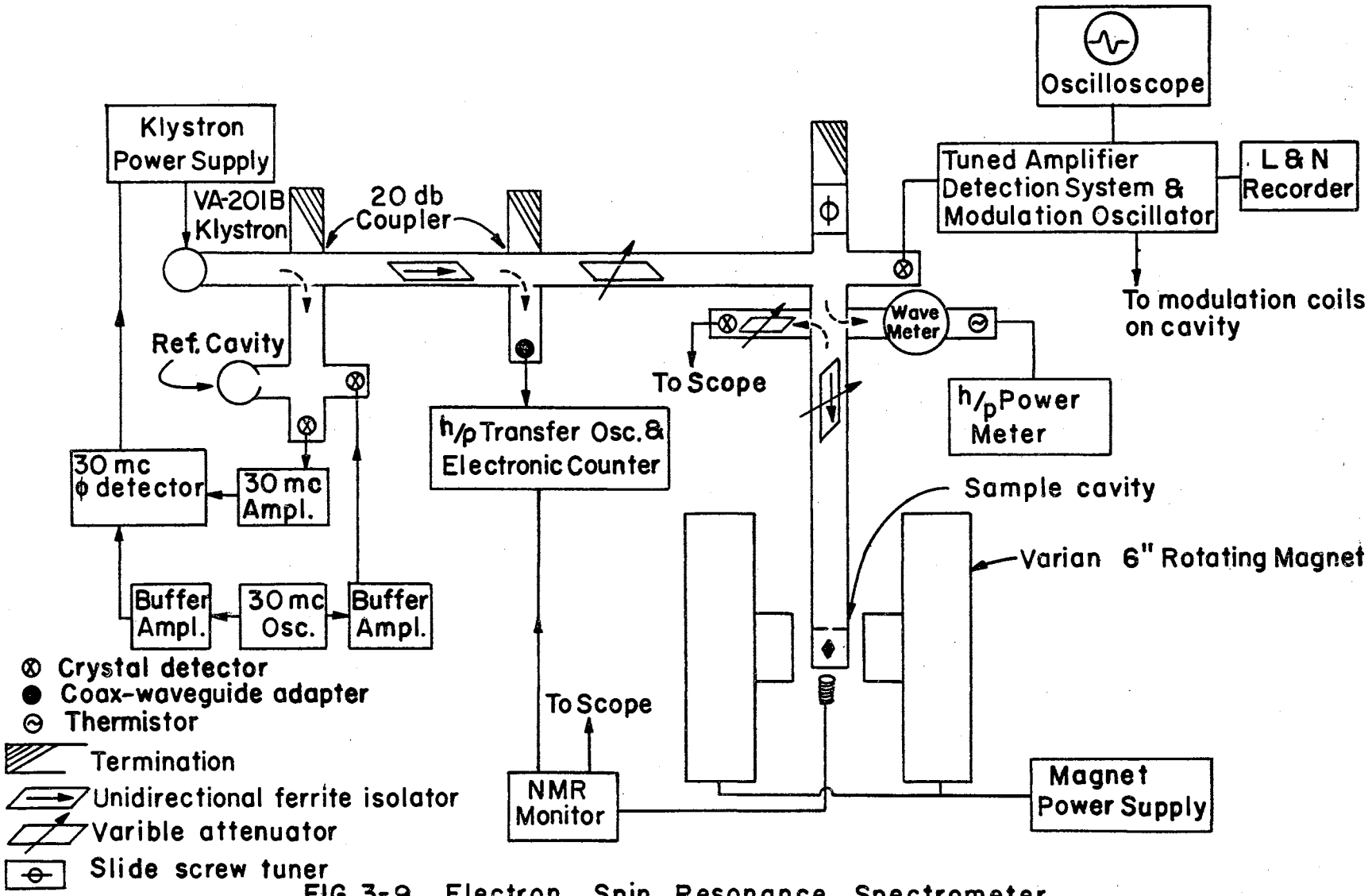

FIG. 3-9 Electron Spin Resonance Spectrometer

incorporates a bidirectional coupler and an adjustable ferrite isolator. The directional coupler in the sample arm allows one to monitor the reflected power from the sample cavity and to measure the power incident on the cavity by using a microwave power meter. Also, the microwave frequency can be measured to the accuracy of a cavity wave meter. The resonance signal is detected in the fourth arm of the bridge using a crystal detector. The signal is then amplified, demodulated in a phase detector, and recorded on a graphic recorder.

The sensitivity of the spectrometer was increased by at least a factor of two by replacing the magic "T" with a microwave ferrite circulator (44). The modified spectrometer is shown in Fig. 3-10. The homodyne circuit configuration is used in order to obtain the correct bias power for the detectors (either bolometers or crystals may be used) (43).

Microwave Cavity

The sample cavity is a very important element in the microwave structure of the ESR spectrometer. The choice between several different cavity structures is dictated by the space available in the magnet gap (low temperature dewars being considered), the size and shape of the sample, the desired Q of the cavity, and the desired microwave magnetic field configuration. Several different cavity structures are shown in Figs. 3-11 and 3-12. Probably the simplest cavity to construct and design is the rectangular TE_{102} cavity. The sample is introduced into the region of maximum microwave magnetic field which is located at the center of the cavity as illustrated in Fig. 3-11. The rectangular cavity has the disadvantage that the microwave magnetic field is in the horizontal plane when placed in the magnet gap, and in studies involving the rotation of the large magnetic

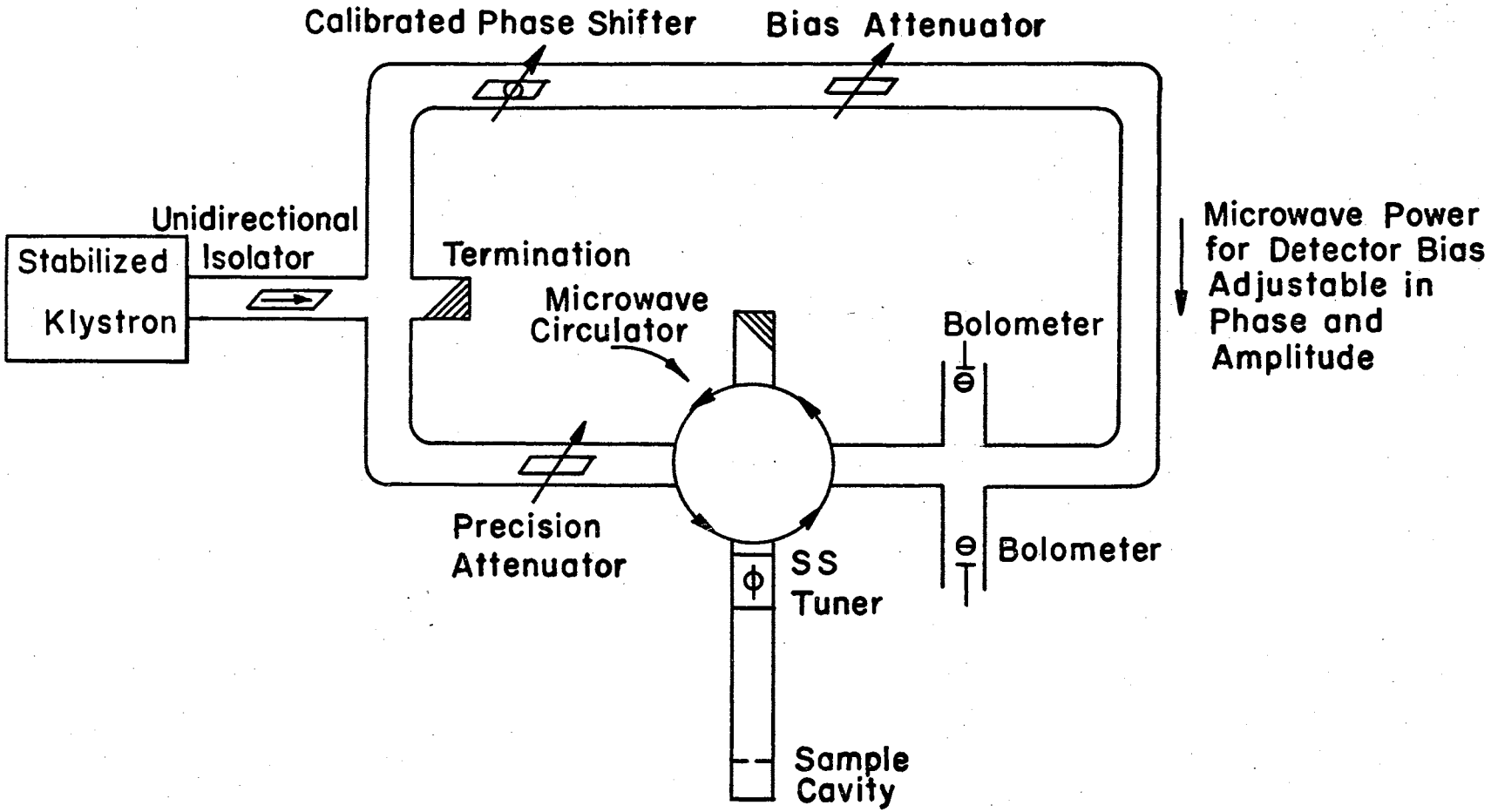

Fig. 3-10 Modification of the Spectrometer Using a Microwave Circulator.

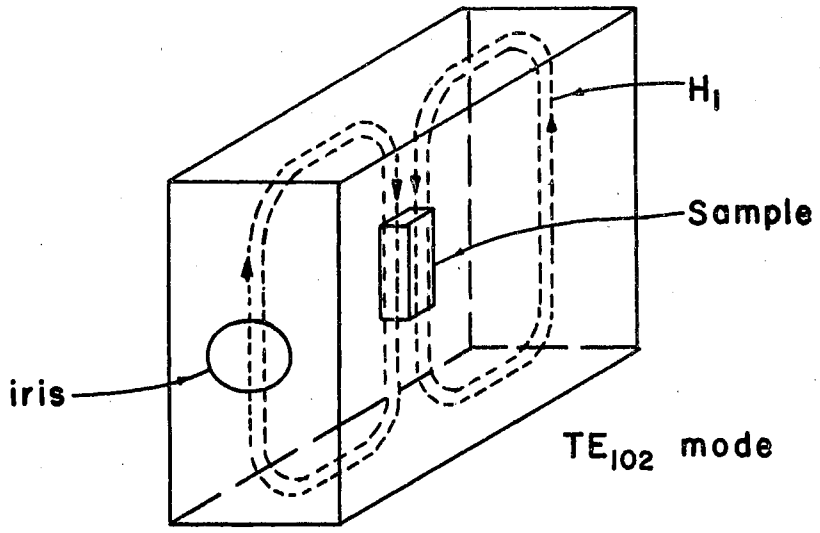

FIG.3-11 Rectangular Sample Cavity. H_1 is the microwave magnetic field. The sample is placed in region of maximum H_1

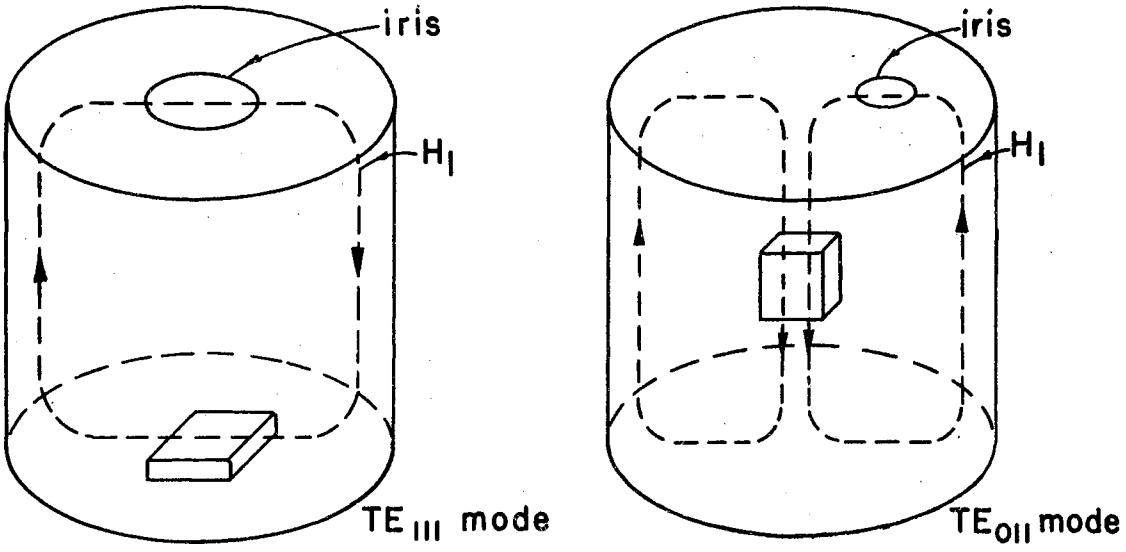

FIG.3-12 Cylindrical cavities showing microwave magnetic field and placing of sample.

field the angle between the large field and the microwave magnetic field is varied which reduces the signal amplitude. In this respect the cylindrical cavity operating in the TE_{011} mode, with its microwave field in the vertical plane, would be more satisfactory. When the Q of the cavity is required to be a maximum the cylindrical structures should be used. Every different sample usually requires a particular cavity structure to satisfy all the measurement requirements; therefore, in most cases, more than one cavity is advantageous. Glass or ceramic cavities have special advantages when high frequency modulation techniques are employed (5). In some of the initial measurements a Varian 100 kc rectangular TE_{102} cavity was used. This Varian cavity allows irradiation of the sample but has the disadvantage of requiring that the sample be rotated instead of allowing the magnet to be rotated. Therefore, we have found that it is necessary to have a variety of cavities available and have constructed a rectangular TE_{102} high frequency cavity with quartz walls and a cylindrical TE_{011} mode cavity made of pyrex with gold plated walls. It should be noted that the TE_{011} cylindrical cavity has a minimum radius of approximately 2 centimeters for x-band operation.

Magnetic Field Measurement

The determination of the magnetic field strength is accomplished using a nuclear resonance detector. The transistor NMR detector of Fig. 3-13 was used initially, but higher sensitivity was obtained from a vacuum tube circuit (45, 46). The transistor circuit is essentially a grid-dip oscillator conveniently reduced in size so it can be mounted directly on the magnet. The NMR probe is rigidly supported with a clamp to the magnet pole piece. The frequency of the NMR oscillator is measured with a h/p 524 D electronic

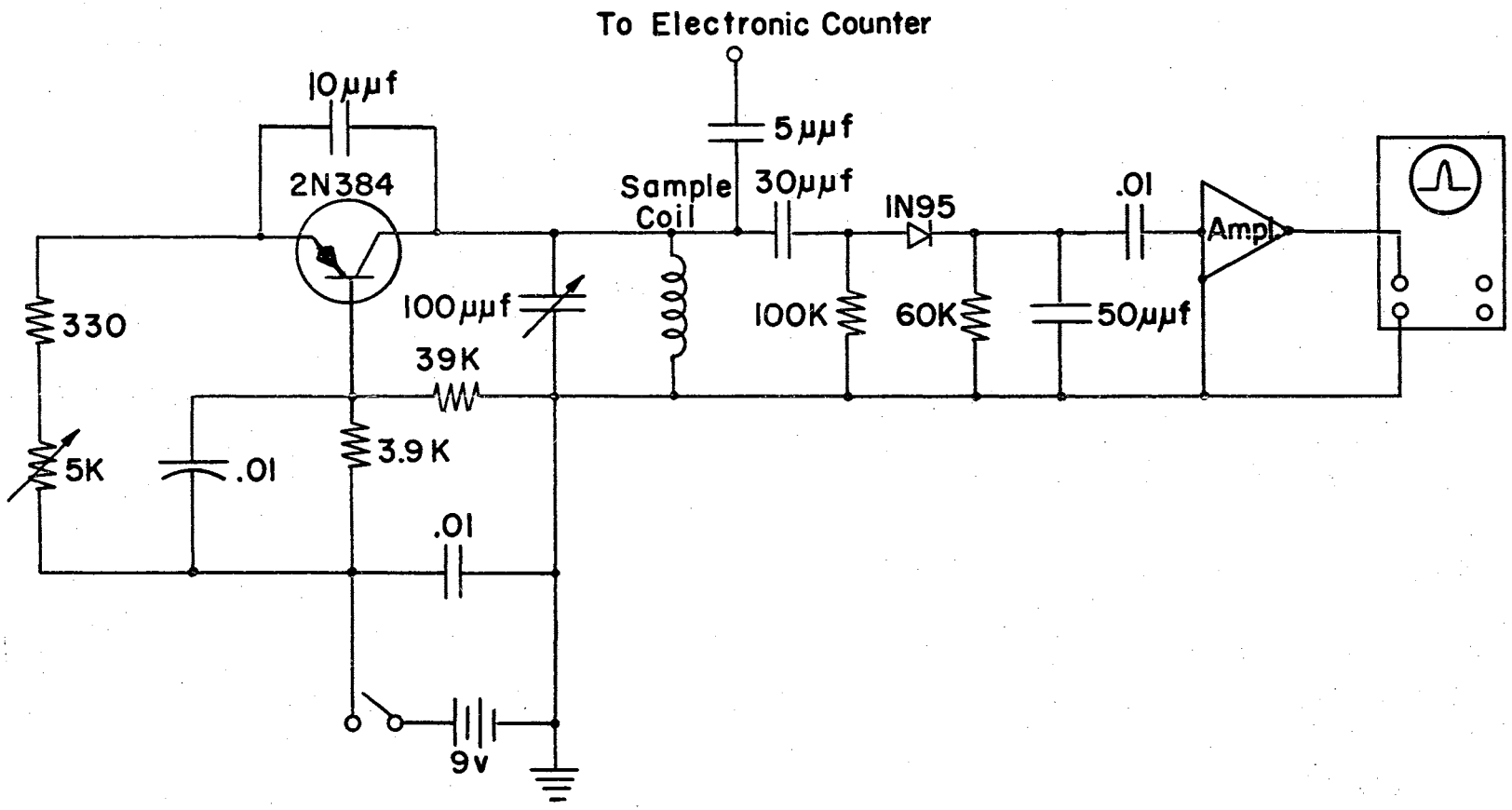

FIG. 3-13 Nuclear Magnetic Resonance Oscillator - Detector

counter. Using the relation $\omega_p = \gamma_p H$ the magnetic field at the probe is given by

$$H = \frac{2\pi\upsilon_p}{\gamma_p} = 2.34868 \times 10^{-4}\ \upsilon_p \text{ (gauss)}$$

where $\gamma_p = 2.67530 \times 10^4$ rad sec^{-1} gauss^{-1} is the gyromagnetic ratio of the protron (47).

Low Temperature Apparatus

The low temperature apparatus consists mainly of the Varian variable temperature and liquid helium equipment. The variable temperature apparatus utilizes the gas flow technique to vary the temperature from -180°C to approximately 300°C. The small quartz dewar fits inside the 100 kc microwave cavity and has the disadvantage of restricting the sample size. Also, the use of the variable temperature apparatus requires the rotation of the sample since the magnet cannot be rotated with the 100 kc cavity in place.

The Varian liquid helium system consists of an inner helium dewar and an outside nitrogen dewar with the stainless steel waveguide and cavity. The waveguide can be evacuated, and a port is available by which the pressure above the liquid helium can be reduced. With proper precautions the temperature of the liquid helium can be reduced below that of the λ -point, but extreme care must be exercised when the system is allowed to warm-up. Below the λ -point the liquid helium creeps into the sealed cavity and a violent explosion can occur if the pressure is not released on raising the temperature. Actually, one should observe this precaution if only liquid nitrogen is used since condensed gases may collect inside the waveguide if a leak occurs. In addition to the Varian system we have the following accessories for liquid helium work:

(1) 25 liter storage dewar (Superior Air Products)

(2) helium transfer tube (Superior Air Products)

(3) helium level indicator (53)

(4) Cartesian manostat (54)

(5) Vacuum system (300 liters/min. free air capacity)

(6) vapor pressure manometer

Summary on the ESR Spectrometer

The microwave ESR spectrometer described is capable of detecting approximately 10^{12} spins (ΔH = 1 gauss and time constant of 10 sec) when used with the Varian 100 kc detection system. The microwave system utilizes a modified Pound discriminator to stabilize the klystron frequency to better than 1 part in 10^6. The magnet system used in the ESR measurements is a Varian 6" rotating magnet with ring-shim pole pieces; however, a current regulating system is described for use with the Varian 4" magnet. Several circuits are given that were constructed for use with the spectrometer. Included in these special circuits is a 30 mc crystal diode phase detector with a dc amplifier, a transistor klystron filament supply, and a low-noise transistorized bolometer amplifier. The ESR spectrometer is capable of being operated at the lower modulation frequencies of 28, 400, and 1000 cps. The magnetic field necessary to produce ESR absorption is measured using a nuclear resonance probe. Accurate frequency measurements of both the microwave frequency and the NMR frequency can be accomplished using a h/p 524 D electronic counter.

CHAPTER IV

RESULTS AND DISCUSSION OF ELECTRON SPIN RESONANCE IN DIAMOND

General Remarks

Remarks on Observations of ESR Parameters to be Discussed

The electron spin resonance spectra of semiconducting diamonds and several insulating diamonds were investigated. The experimental parameters determined from the measurements on semiconducting diamonds include the g-factor, line width, and number of unpaired spins. In the measurements on semiconducting diamonds the temperature was varied from $108^{o}K$ to approximately $370^{o}K$ and some experimental work was done at $4.2^{o}K$. A diamond was crushed and exhibited an ESR line similar to that observed in semiconducting diamonds. Changes of the ESR absorption in the crushed diamond were observed upon heat treatment. The colored diamonds investigated exhibited complex ESR spectra, and the resolution of structure was extremely directional dependent in some specimens. Optical transmission measurements in the infrared were made on most of the diamonds investigated by the ESR method.

Description of the Diamonds

The semiconducting diamonds used in this investigation are a natural blue color, sometimes referred to as steel-blue, with the exception of

DS-5 which has a brownish tinge added to the usual blue color[2]. The diamond DS-1 has an irregular shape with some natural (111) faces that are easily identifiable; DS-1 is one of the better semiconductors ($\rho \cong 50$ ohm-cm at room temperature) and was referred to in earlier work as the "Chip". Diamond DS-2 had been cut and polished in the shape of a rectangular parallelepiped measuring 2.5 x 3.5 x 6.5 mm^3. This particular diamond has received a more intensive investigation of its properties than the other semiconducting diamonds (48). One end of DS-2 is blue, extending about 1.4 mm into the diamond, and the other end is clear as distinguished with the eye. The third semiconducting diamond is a gem stone with a marquise cut and is referred to as DS-3. DS-3 is perhaps the bluest of the diamonds investigated. A fourth diamond, DS-4, was only available for a short time, and very little data were obtained on it. The largest of the semiconducting diamonds, DS-5, has two parallel (111) faces that make it convenient for optical transmission measurements. The semiconducting diamonds have the following weights:

Diamond	wt. (gms)
DS-1	0.0787
DS-2	0.1726
DS-3	0.1130
DS-5	0.7375

The insulating diamonds investigated were mostly Type I, but a Type IIa was found among the diamonds in our collection of triangular flats. Some of the diamonds are visibly colored; the colors being a clear yellow,

[2]Semiconducting diamonds herein are denoted by DS; whereas, ordinary insulating diamonds are designated using the letter D. Clarification of this notation with that used in earlier work on the same diamonds will be noted where it is necessary.

yellow, green, brown, and yellow-green. The insulating diamonds vary in weight from 0.1 gm to approximately 0.01 gm. The series of five diamonds D-62 to D-66 are colored yellow to dark brown and exhibited a cubic growth habit. Most of the diamonds have recognizable natural faces.

ESR Parameters Associated with Paramagnetic Defects

The g-factor is defined by the fundamental relationship $h\upsilon = g\beta H$. An expression that is used in the determination of the g-factor, using an organic free radical as a reference, can be deduced from this relationship. The desired expression is obtained from $h\Delta\upsilon = g\beta\Delta H + \beta H\Delta g$ for $\Delta\upsilon = 0$, i.e., at a constant microwave frequency. The g-factor of the unknown diamond sample is given by

$$g_s = g_f \left(1 - \frac{\Delta H_o}{H_f}\right) \qquad (4.1)$$

where f refers to the known value of g and H for the free radical, and ΔH_o is the magnetic field interval between the observed resonance lines. The free radical diphenyl-picryl-hydrazl (DPPH) has a g-factor equal to 2.0036 ± 0.0003 (1). The unknown g-factor is determined by measuring the magnetic field scanning rate and the microwave frequency. The magnetic field for the DPPH free radical resonance is given by

$$H_f = \frac{\upsilon_f}{2.80724} \text{ gauss} \qquad (4.2)$$

where υ_f is the microwave frequency, measured in megacycles using a cavity wavemeter. The reference g-marker is usually inserted into the sample cavity with the diamond in place so that the microwave frequency is not changed during the measurement. The magnetic field interval is determined by measuring the scanning rate of the magnetic field. As the magnetic

field is scanned it is monitored using a nuclear resonance probe, with markers being placed on the recorder chart at regular intervals. The frequency of the nuclear resonance oscillator is determined with an electronic counter and the corresponding magnetic field is calculated as described in the section on magnetic field measurements.

The width of the ESR absorption line can be conveniently measured between points of maximum and minimum deflection on the derivative curve if a modulation detection system is used. If the modulation amplitude is very small compared to the line width, $H_m \cong 0.1\ \Delta H$, then the width can be measured directly. Microwave power to the sample must be small so that saturation of the resonance line does not occur during this measurement. However, under extremely low signal-to-noise ratios the condition of small modulation amplitude is very difficult to obtain, and the amplitude of modulation must be increased to improve the signal strength. Over-modulation of the resonance line has a broadening effect that can be corrected for by extrapolation to zero modulation amplitude provided the condition $H_m < \Delta H$ is observed (49). If $H_m \gg \Delta H$ the peak-to-peak distance on the derivative curve becomes equal to $2H_m$ (50).

Another parameter that has proven to be useful in the interpretation of paramagnetic defects in the solid state is the total number of unpaired spins or the spin concentration. The total number of unpaired spins in the diamond specimen can be determined using DPPH as a standard. Such a determination involves the measurement of the first moment M_1 of the derivative curve since it is proportional to the intensity of absorption

$$I \propto \int_{-\infty}^{\infty} g'(h)\ h\,dh \qquad (4.3)$$

where $g'(h)$ is the approximate derivative of the absorption curve as recorded, and the integral is the definition of the first moment. It is necessary to evaluate the integral graphically or by using an analogue technique. The method used involves the determination of the first moment of a reference sample under the same experimental conditions as used to obtain the first moment of the ESR line in diamond (52). In case the same experimental conditions are not observed, the following corrections need to be considered: (a) changes in the cavity matching, (b) degradation of the cavity Q, (c) microwave power level variations, (d) modulation amplitude, and (e) amplifier gain. The DPPH reference sample was inserted into the cavity with the diamond so that the simple expression

$$N_s = N_f \frac{M_{1s}}{M_{1f}} \frac{A_f}{A_s} \tag{4.4}$$

could be used to determine the number of unpaired spins, N_s, in the diamond specimen. M_{1s} and M_{1f} are the measured first moments from the diamond and free radical resonance curves, respectively. In general, only the gain of the amplifier was changed and this is corrected for in equation (4.4) by the ration A_f/A_s . N_f is the total number of spins in the free radical DPPH (mol. wt. = 394).

Results of Measurements on Semiconducting Diamonds

g-Value, Line Width, and Number of Unpaired Spins

A single electron spin resonance line was observed in all the semiconducting diamonds investigated. Figure 4-1 shows a typical curve characteristic of these diamonds. The g-factor, line width, and number of spins was determined for the diamonds DS-1, DS-2, and DS-3, but only limited measurements were obtained on DS-4 and DS-5. The ESR parameters were

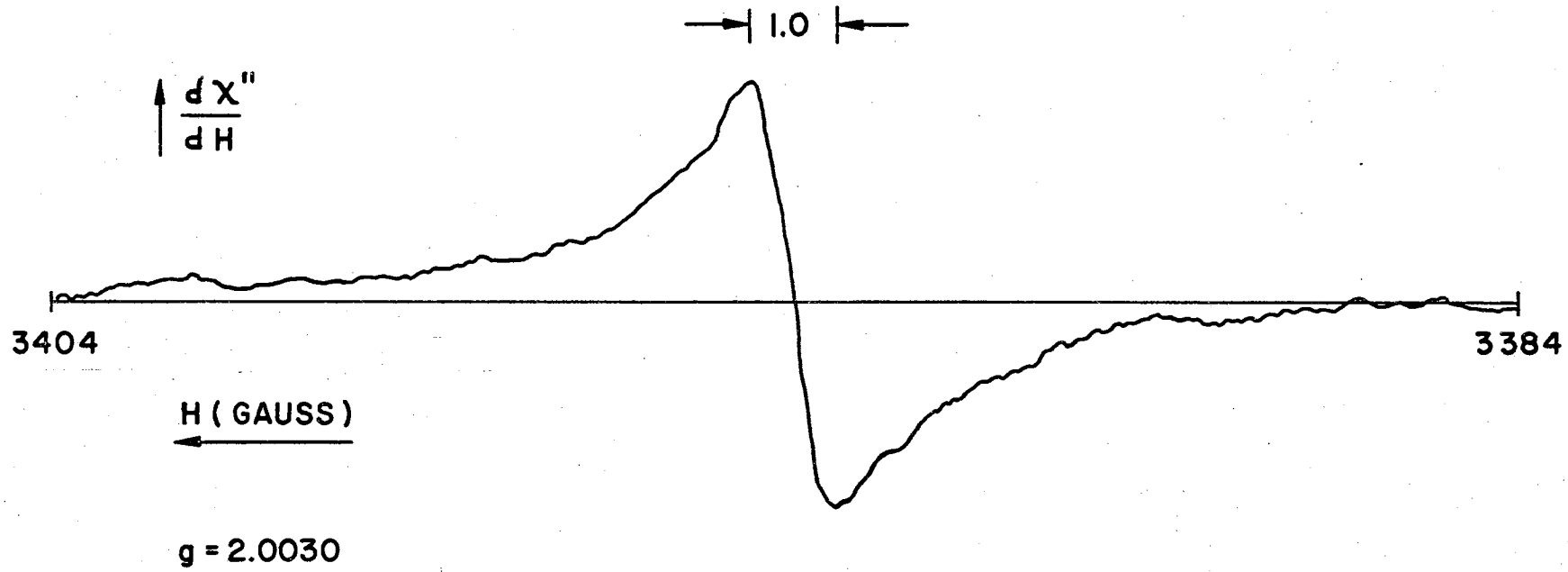

ELECTRON SPIN RESONANCE in SEMICONDUCTING DIAMOND

DIAMOND DS-3

TEMPERATURE 25° C

FIG. 4-1

calculated using the techniques as described in the preceding section.

The g-factor of the diamonds investigated varied from 2.0014 to 2.0040 at room temperature, with semiconducting diamonds having the larger positive g-shift (Δg) from that of the free electron (g=2.0023). Measurements of the g-factor were taken at lower temperatures, but no significant changes took place until the temperature was reduced to that of liquid helium. The g-factor of DS-5 was measured at 4.2°K and found to be 2.01. In general, the g-factor did not change with crystal orientation. Table II shows the measured g-factor for the different semiconducting diamonds. All measurements were taken at room temperature except where noted.

TABLE II

g-VALUE OF ESR LINE IN SEMICONDUCTING DIAMONDS

Diamond	g (±0.0003)	$\Delta g \times 10^4$
DS-1	2.0028	+5
DS-2	2.0031	+8
DS-3	2.0030 2.0031 (131°K)	+7
DS-4	2.004	---
DS-5	2.0027 2.01 (4.2°K)	+4

The width of the resonance line in semiconducting diamond varied from 0.3 to 8 gauss for different specimens when measured at room temperature. The line width decreased when the temperature was lowered indicating a fairly strong temperature dependence. Saturation measurements could not

be made because of insufficient microwave power; however, an estimate of the spin-lattice relaxation of 10^{-9} seconds was obtained for the diamond DS-3 at 108°K. As in the measurements on the g-factor, the line width was found to be isotropic. Table III lists the line widths and the temperature at which they were measured. Also listed in this table is the total number of unpaired spins in three of the semiconducting diamonds.

TABLE III

LINE WIDTH AND NUMBER OF UNPAIRED SPINS IN SEMICONDUCTING DIAMONDS

Diamond	Line Width (ΔH) in gauss 298°K	140°K	Total Number of Unpaired Spins (N_s)
DS-1	8.3	6.9	4.1×10^{14}
DS-2	2.7	2.0	5.1×10^{13}
DS-3 (a)	1.0	0.2	3.4×10^{13}
DS-4	1.6	-	-
DS-5	0.3	-	-

(a) The line width of DS-3 is 1.8 gauss at 370°K

The total number of unpaired spins rather than the density of spins is listed for the semiconducting diamonds DS-1, DS-2, and DS-3 because the distribution of spin centers is unknown. With this point in mind the total number of spins is considered the more important factor. If a uniform distribution is assumed the spin density is 2×10^{16}, 1×10^{15}, and 1×10^{15} spins per cc for DS-1, DS-2, and DS-3; respectively. The paramagnetic susceptibility was found to vary as 1/T in the temperature range 108°K - 298°K for the diamond DS-3.

ESR Measurements at 4.2°K

Electron spin resonance was detected in only one of the semiconducting diamonds, DS-5, at 4.2°K. The resonance absorption was detected under rapid passage conditions (57) and is shown in Fig. 4-2. Unresolved structure appears on the sides of the main resonance line due to interaction with a nucleus of non-zero magnetic moment, presumably C^{13}. A slight reorientation of the diamond gave better resolution of the side peaks and the splitting from the central line was found to be approximately 5 gauss. The splitting is close to the value obtained by Baldwin (24) who investigated the ESR spectrum of an electron-irradiated Type IIa diamond. The splitting was interpreted as the interaction of the unpaired spin with the vacancy second-nearest-neighbor C^{13} nuclei. There is doubt as to the exact orientation of the specimen, consequently the question of anisotropy is unanswered at the temperature of 4.2°K. A resonance line was not detected in DS-1, DS-2, or DS-3; however, further work at liquid helium temperature is needed in order to verify this result.

Infrared Transmission Measurements

Infrared transmission measurements were made at room temperature on the diamonds DS-1, DS-2, DS-3, and DS-5 using a Beckman IR-7 spectrophotometer. The infrared optical properties of the diamonds are characteristic of semiconducting diamonds, i.e., absorption occurs at 3.42, 3.57, and 4.07 μ. In addition, the diamonds show absorption at 7.5 μ (1332 cm^{-1}) and 7.8 μ. Also, several absorption peaks occur in DS-5 and DS-3 that are not detected in the other semiconducting diamonds. The peaks that occur in semiconducting diamonds and are considered unusual for this type of diamond include the following:

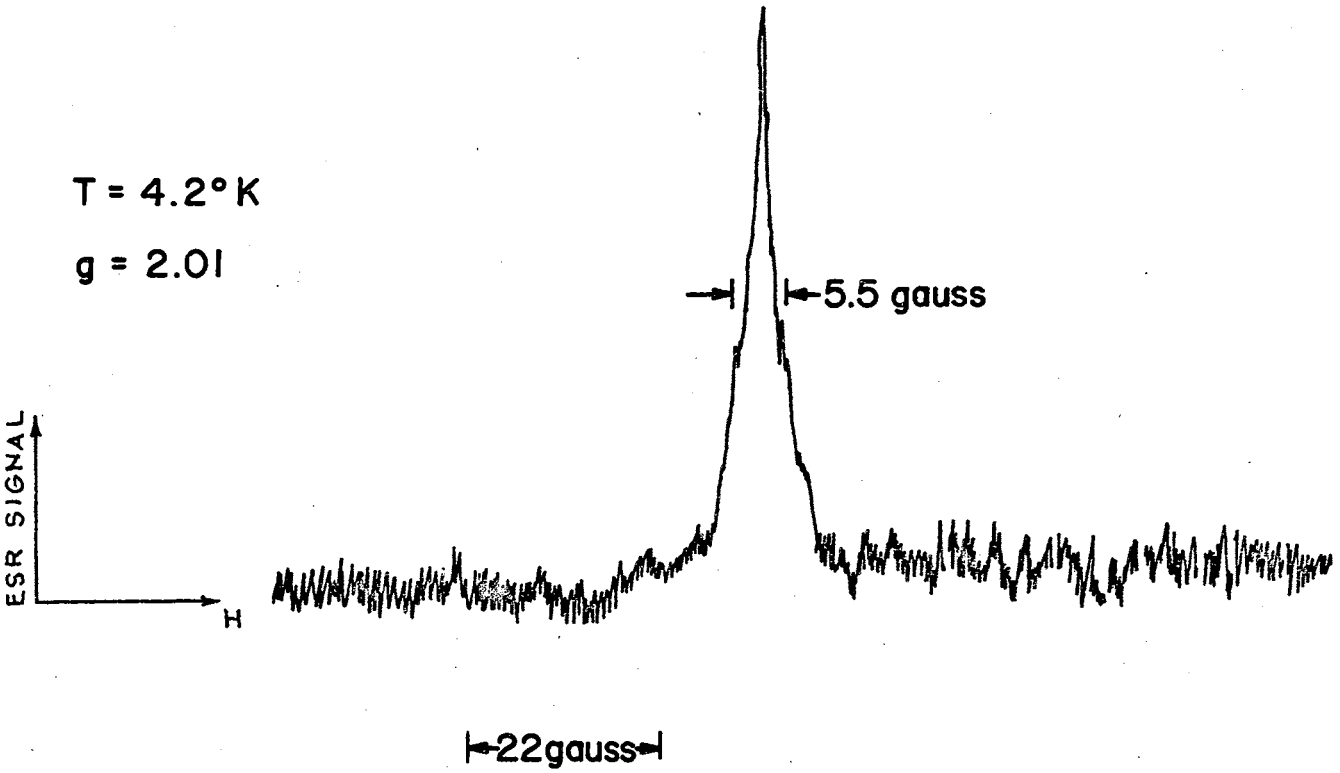

ELECTRON SPIN RESONANCE IN SEMICONDUCTING DIAMOND DS-5

FIGURE 4-2

DS-5	DS-3
6.07μ broad line	---
6.85μ weak	---
7.50μ fairly strong (B)	7.50μ weak (B)
7.80μ strong (A)	7.80μ weak, broad (A)
8.63μ weak, broad (B)	8.6 μ weak (B)
9.0 μ weak (A)	9.0 μ very weak (A)
11.9 μ (B)	---
13.4 μ (B)	---

The absorption coefficient could not be accurately determined on these diamonds; however the detectable differences in the 7.8μ region are shown in Fig. 4-3. The 7.8μ band has been previously detected in semiconducting diamond (55, 56), but no indication of the 7.5μ absorption appeared. The A and B absorption peaks refer to the impurity centers found in ordinary diamond (6).

ESR in Diamond Due to Mechanical Damage

Effects of Heat Treatment

Paramagnetic centers were produced in a Type I diamond by mechanically crushing the specimen in a steel mortar. The diamond, D-17, was selected for this experiment because it was clear in color and showed no spin resonance absorption before crushing. The diamond has an easily detectable absorption at 7.8μ, an ultraviolet cut-off near 300 mμ, and displayed a strong luminescence on irradiation with ultraviolet light.[3]

[3]The ultraviolet cut-off and luminescence was determined by C. C. Johnson in a survey of fifty triangular flat diamonds at OSU.

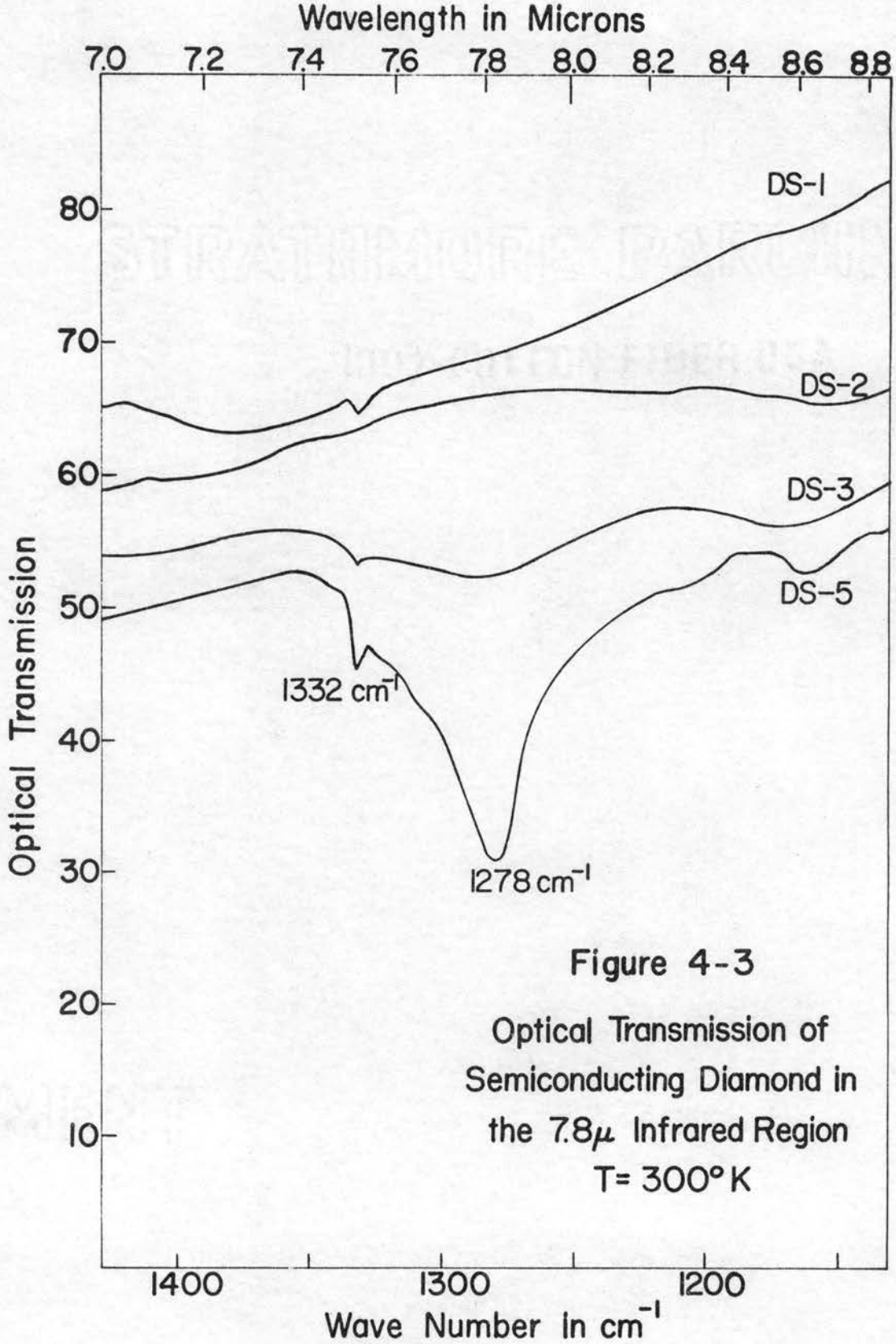

Figure 4-3

Optical Transmission of Semiconducting Diamond in the 7.8μ Infrared Region T= 300° K

After crushing, the diamond was cleaned in warm aqua fortis (2/3 H_2 SO_4 and 1/3 HNO_3) for thirty minutes followed by a similar treatment in nitric and hydrochloric acid. The acid was removed and the crushed diamond was rinsed in distilled water. The crushed diamond was then transferred to a quartz tube and evacuated to a pressure of 10^{-6} mm Hg.

The ESR absorption observed in crushed diamond is similar to that observed in the semiconducting diamonds. The g-factor is 2.0029, and the line width of the crushed diamond before heat treatment was 2.9 gauss. The effects of heat treatment in a vacuum are negligible for a temperature below 500°C. However, the intensity of the original line is reduced considerably after heating for just one hour at 600°C. The signal continued to decrease as the temperature was raised to 780°C. The resonance absorption did not continue to decrease with heat treatment but reached a constant value and remained after heat treatment at 1100°C for 4 hours. The line width decreased to 1.6 gauss after a heat treatment to 960°C. In addition to the narrow line, a broad line occurred after a heat treatment temperature of 870°C for one hour.

Another diamond (D-39), exhibiting a single resonance line, was used as a control specimen for the heat treatment experiments. No change of this line occurred during the heat treatment, nor was there any change in the infrared spectrum. D-39 had a very slight absorption in the infrared at 7.8μ and an ultraviolet cut-off of 225 mμ.

ESR in Type I Diamond

Nitrogen Resonance in Type I Diamond

In the present investigation a 3-line spectrum[4] was observed in a series of five Type I diamonds exhibiting the cubic growth habit: D-62 through D-66. The 3-line spectrum has been attributed to nitrogen (21) with the intensity ratio of 1:1:1 and a splitting between the outer lines of approximately 70 gauss. The same ESR line is observed in the cubic diamonds with the intensity of absorption increasing as the color of the diamonds varies from yellow to dark brown. The resonance line due to nitrogen is more easily saturated then the ESR line in semiconducting diamond. Also, no evidence for exchange narrowing of the nitrogen resonance line is observed. The line width, ΔH, of two of the cubic diamonds was measured and are listed below along with the concentration of spins, N_c. The concentration of spins was calculated assuming a dipolar broadening and a uniform distribution of spins (2).

Diamond	ΔH (gauss)	N_c (per cc)	Color
D-63	0.8	4×10^{18}	yellow-brown
D-66	2.8	1.4×10^{19}	dark brown

In addition to the nitrogen resonance, we have observed a 3-line spectrum in a yellow diamond, D-51B, having an intensity ratio of 1:2:1. The resonance lines are shown in Fig. 4-4, where the splitting between the outside lines and the central line is 34.4 gauss when the $\langle 100 \rangle$ direction is parallel to the magnetic field. The angular dependence of the spectrum is the same as observed for the nitrogen resonance (21). It should be noted that extremely sharp infrared absorption occurs in this diamond at

---

[4]The 3-line spectrum occurs when the $\langle 100 \rangle$ direction is parallel to the applied magnetic field.

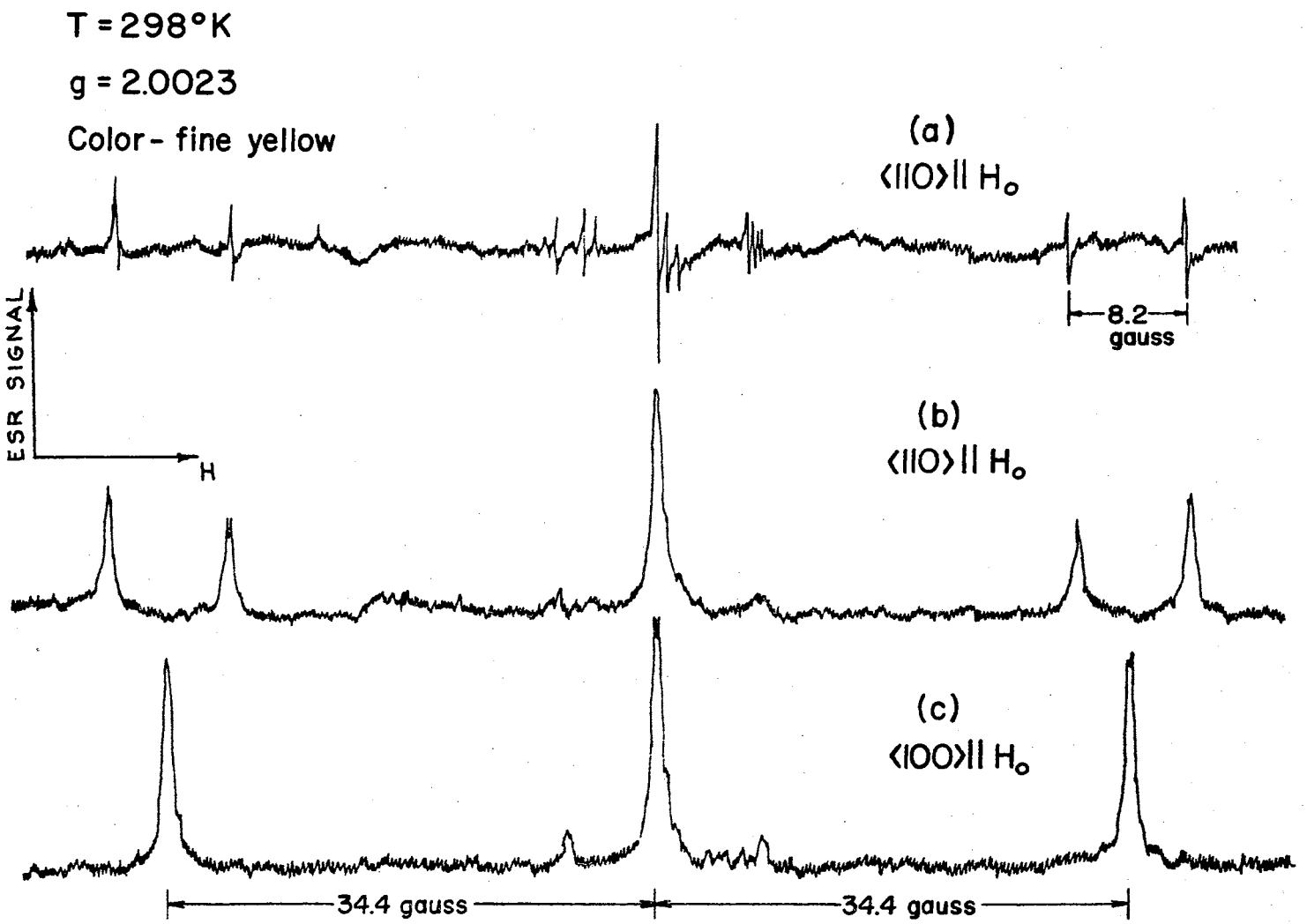

Fig. 4-4 Electron Spin Resonance in Diamond D-51B.

3.2 and 7.1 μ (3107 and 1405 cm^{-1}). The g-factor of this ESR line is 2.0023 and the line width is 0.1 gauss. Extra lines occur in D-51B, as shown in Fig. 4-4a, near the central line. The particular spectrum found in D-51B has been observed in one other diamond, D-58.

Complex ESR spectra in Brown, Yellow, and Green Diamonds

A complex ESR absorption spectrum occurs in several colored diamonds. Figure 4-5 shows a typical spectrum observed in a green diamond, D-57. There appear to be 13 lines with a splitting between the lines of approximately 1.6 gauss when the ⟨100⟩ direction is parallel to the magnetic field. The angular dependence and an accurate analysis would be difficult because of overlapping lines. In a light yellow-green diamond, D-52A, the spectrum of Fig. 4.6 is observed; the major difference from that observed in D-57 being in the extra lines split off from the main spectrum by about 34 gauss. The outer lines in D-52A are single when the magnetic field is parallel to the ⟨100⟩ or the ⟨110⟩ direction, but splits into two components when the ⟨111⟩ axis is parallel to H_o. The g-factor has not been accurately determined but lies very close to the free electron value.

In brown diamonds the spectrum of Fig. 4-7 is observed at g = 2.0024. In addition to the complex spectra obtained from measurements of ESR in yellow and green diamonds, there appears a very sharp central resonance line and, also, two lines occur when the magnetic field is parallel to the ⟨100⟩ direction. The total splitting between the outside lines is 70 gauss, with each line being approximately 35 gauss from the center line. The intensity of the side lines decreases in the ⟨111⟩ direction (rotation in the (110) plane) and is zero when H_o is parallel to the ⟨110⟩ direction, as shown in Fig. 4-7. This spectrum is not an isolated case, but is

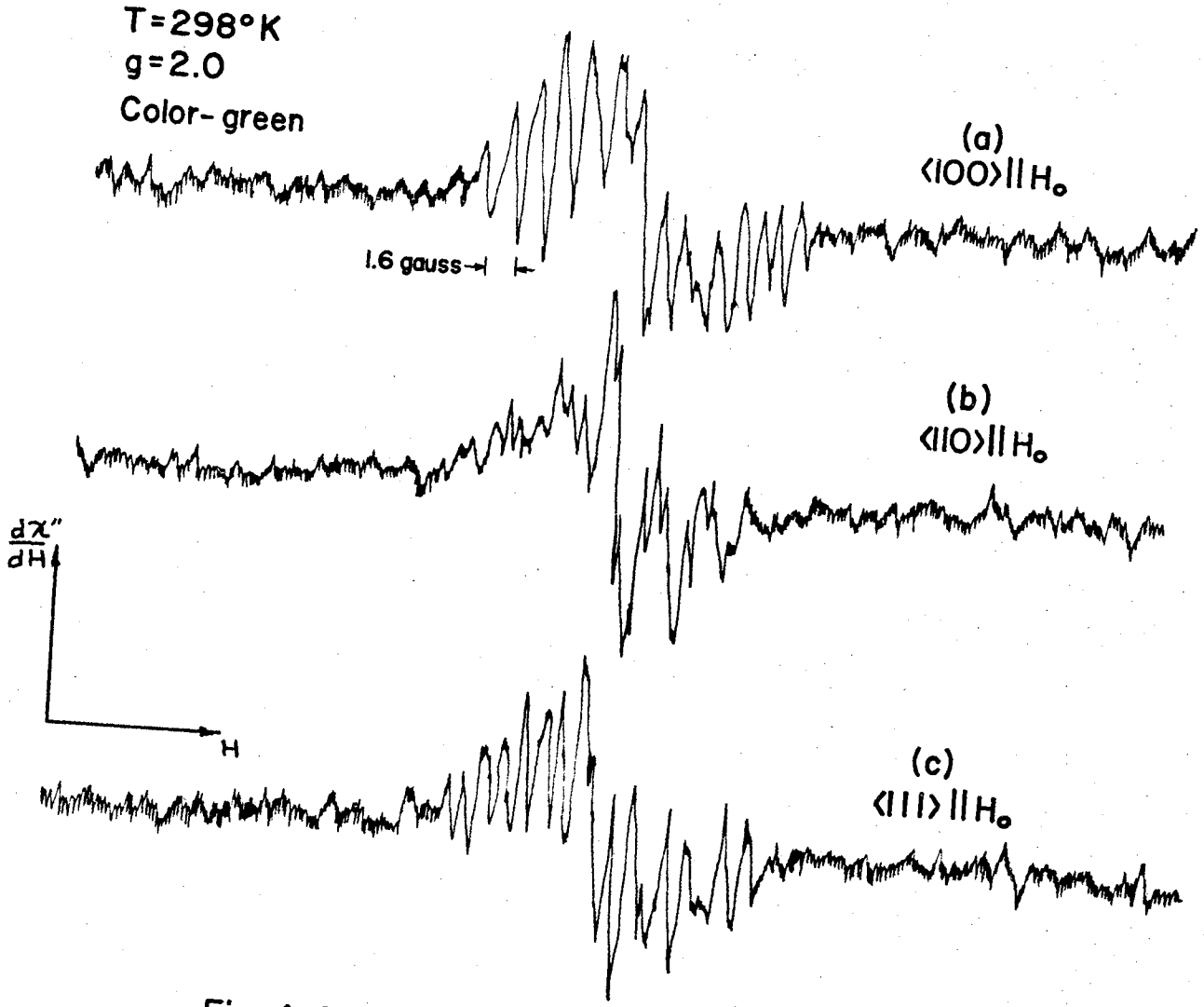

Fig. 4-5 Electron Spin Resonance in Diamond D-57.

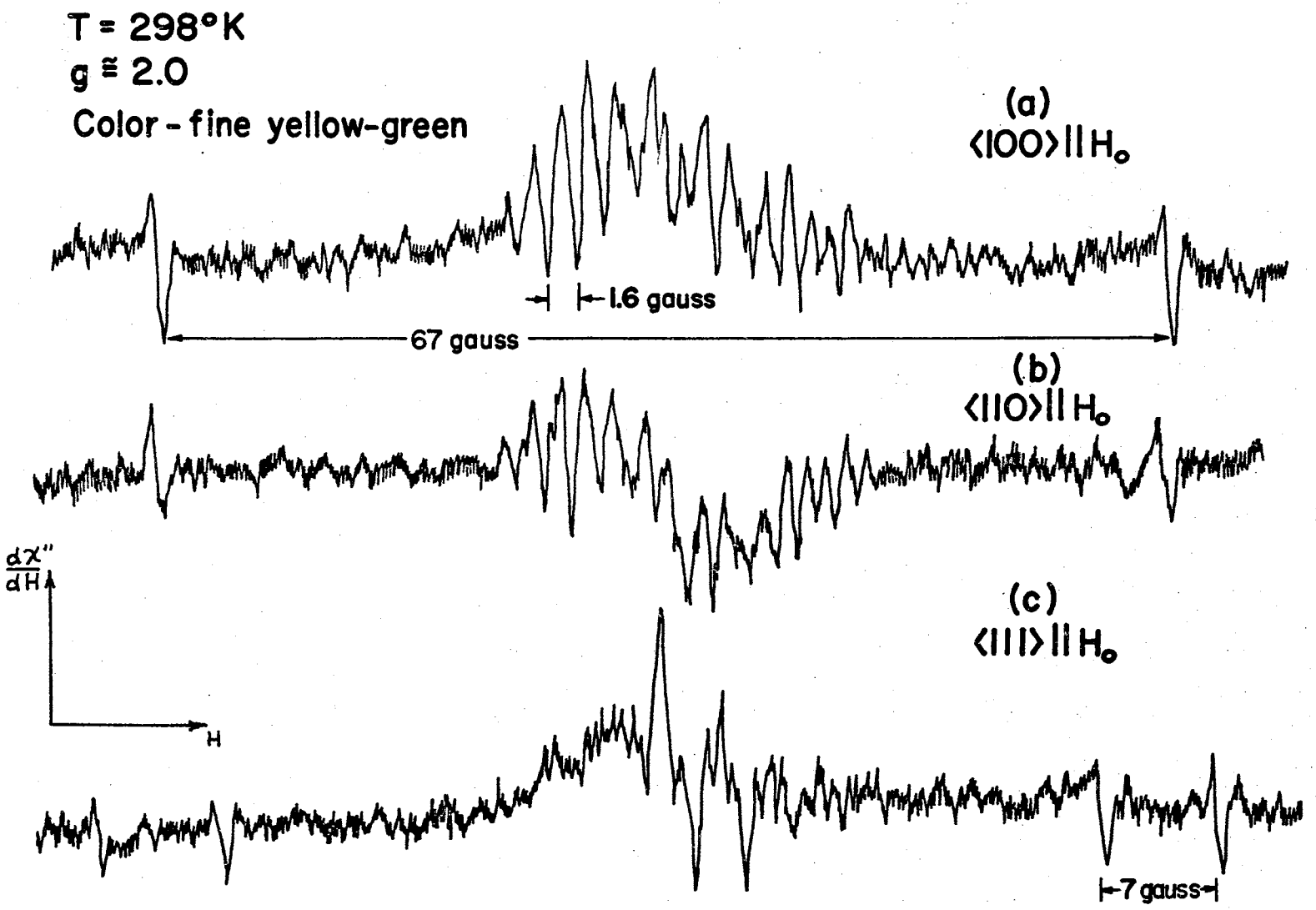

Fig. 4-6 Electron Spin Resonance in Diamond D-52A.

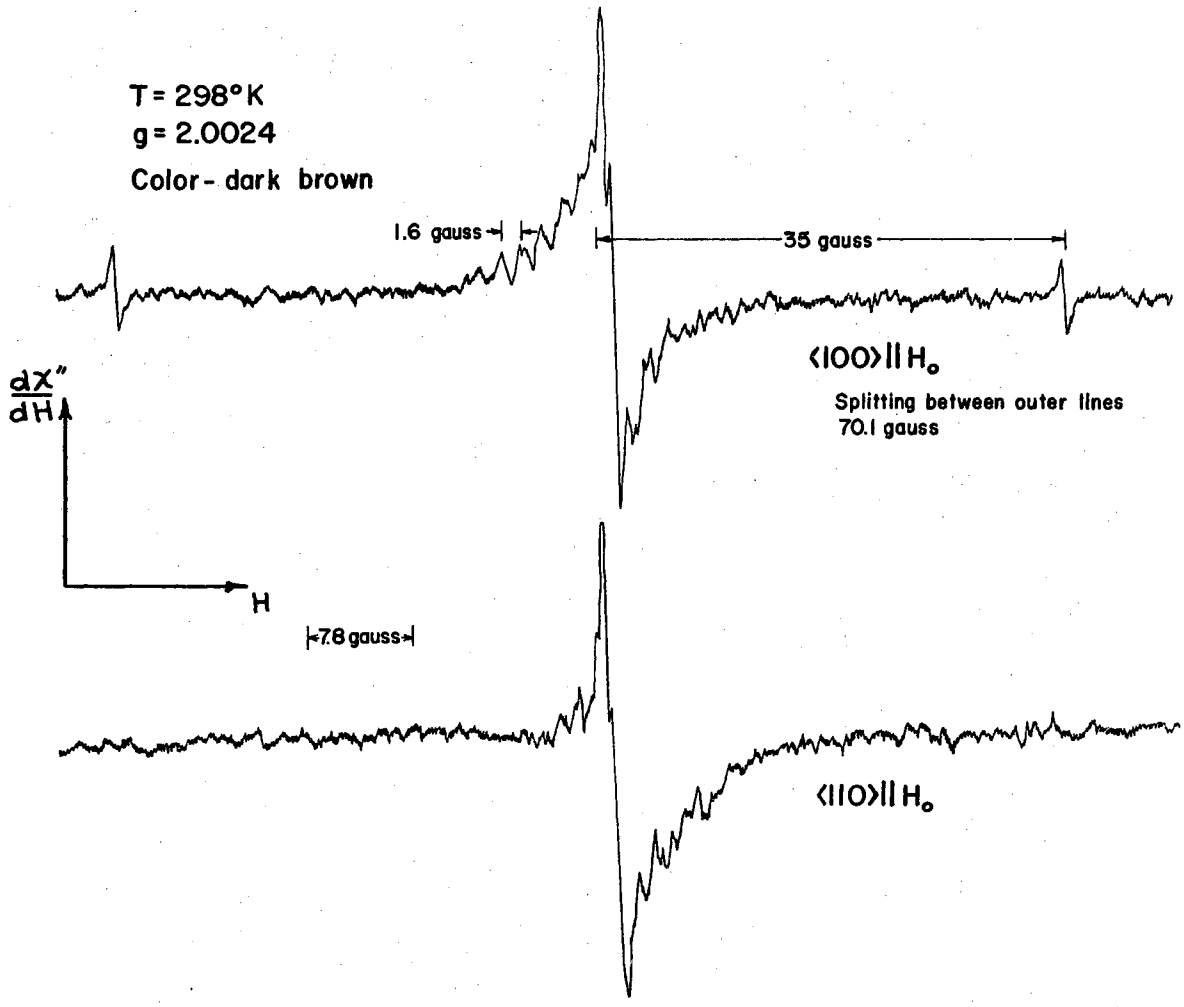

Fig. 4-7 Electron Spin Resonance in Diamond D-61

observed in other brown diamonds having similar physical characteristics (D-54A and D-60). The diamonds were probably grown under similar environmental conditions that accounts for their apparent similarity.

Infrared Transmission of Type I Diamonds

The infrared transmission of the insulating diamonds was measured, as in the case of the semiconducting diamonds, with a Beckman IR-7 spectrophotometer. Figures 4-8 and 4-9 show the results obtained for several of the Type I diamonds.

The diamond cubes D-62 through D-66 have a characteristic infrared transmission spectrum as shown for D-66 in Fig. 4-8. The sharp absorption peaks at 2.87, 3.02, 3.18, 3.22, 6.07, 7.12, 7.34, 7.40 and 7.43 μ seem to be associated with the ESR line, although a quantitative relationship was not determined. Noticeable structure is covered by the continuous absorption from 7.5 to 9.1 μ.

The diamonds D-50B, D-51B, and D-52B could be separated according to their yellow color; however, significant differences occur, not only in the ESR spectra, but in their infrared characteristics as shown in Fig. 4-8 and Fig. 4-9. D-51B is a relatively clear yellow diamond and has very sharp absorption peaks at 3.2, 7.1, and 6.07 μ (3107, 1652, and 1405 cm^{-1}). The absorption at 3.2 μ is readily detectable in the diamonds showing these peaks, even if the long wavelength peaks are covered by other absorption maxima.

All the diamonds showing strong absorption at 7.3 μ have similar complex ESR spectra; these include the yellow, brown, and green diamonds.

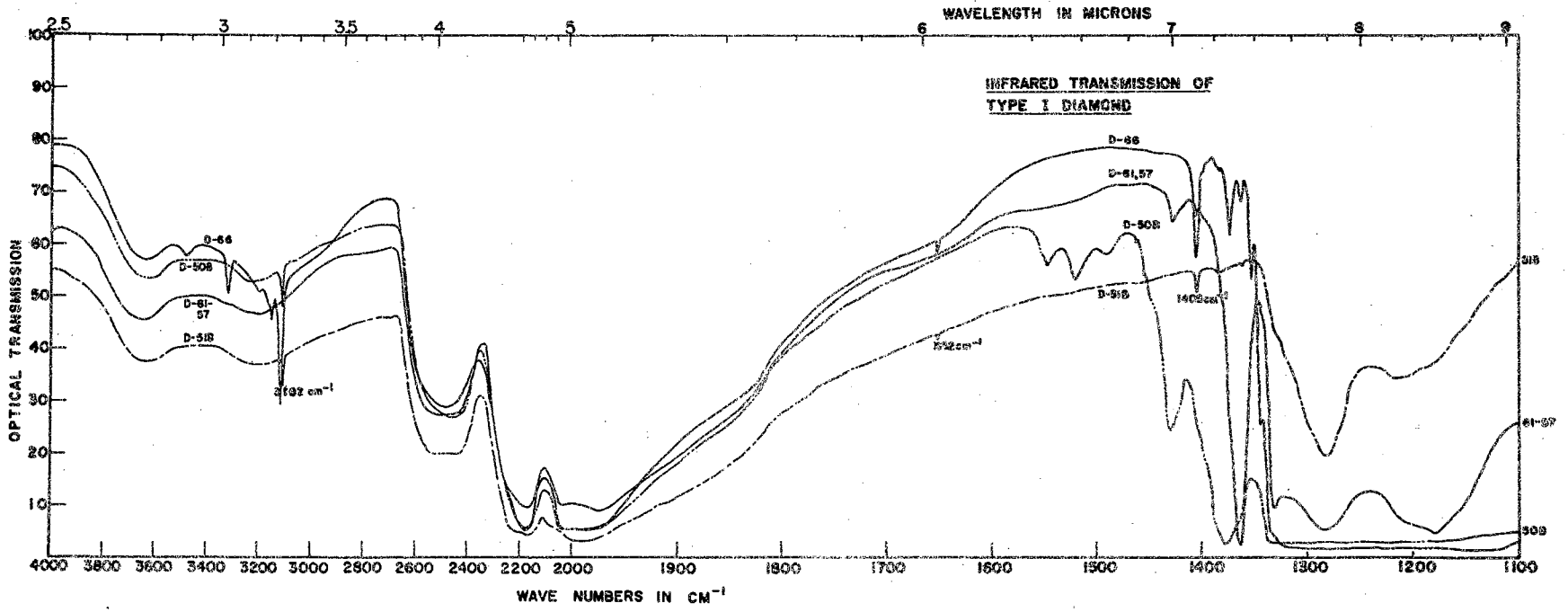
WAVELENGTH IN MICRONS
2.5
3
3.5
4
5
6
7
8
9
INFRARED TRANSMISSION OF
TYPE I DIAMOND
D-66
D-61,57
D-508
D-518
OPTICAL TRANSMISSION
100
90
80
70
60
50
40
30
20
10
4000
3800
3600
3400
3200
3000
2800
2600
2400
2200
2000
1900
1800
1700
1600
1500
1400
1300
1200
1100
WAVE NUMBERS IN CM⁻¹

Figure 4-8

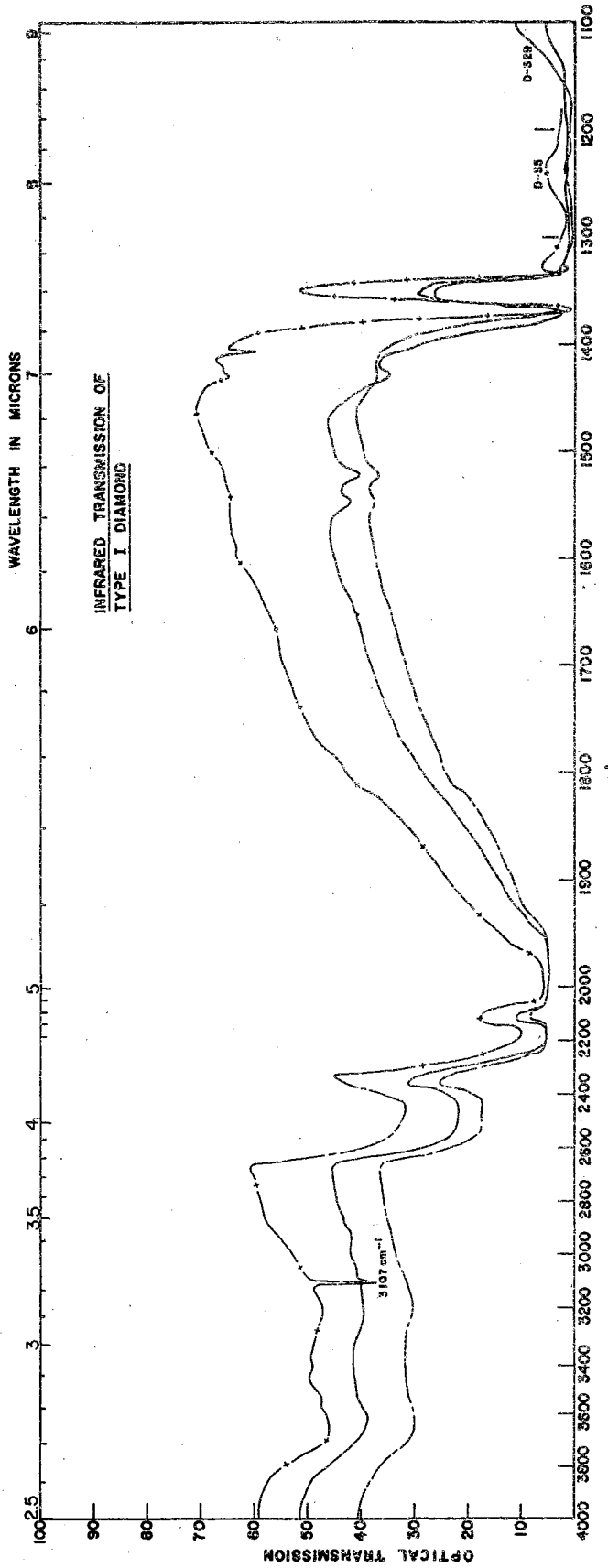
INFRARED TRANSMISSION OF
TYPE I DIAMOND
WAVELENGTH IN MICRONS
WAVE NUMBERS IN CM⁻¹
OPTICAL TRANSMISSION
3107 cm⁻¹
D-329
D-95

Figure 4-9

DISCUSSION

Nature of the Paramagnetic Centers in Semiconducting Diamonds

The ESR spectrum of all the p-type semiconducting diamonds investigated consisted of a single resonance peak at room temperature. The resonance line found in these diamonds has the following general properties:

(1) The g-factor is isotropic and has a value of 2.0030 at $298^{\circ}K$.

(2) The total number of spins is of the order of 10^{14}.

(3) The line width varies from 0.3 to 8 gauss at $298^{\circ}K$ for various diamonds. The width is isotropic and decreases with lower temperatures.

(4) The spin center is associated with the infrared absorption at 7.8 μ.

(5) The spin-lattice relaxation time (T_1) is approximately 10^{-9} seconds.

(6) Resolved structure at $4.2^{\circ}K$ is probably due to the interaction with C^{13} nuclei.

Table IV gives a summary of the information obtained from measurements on semiconducting diamonds at room temperature.

TABLE IV

SUMMARY OF RESULTS ON SEMICONDUCTING DIAMONDS

Diamond	N_s	g	ΔH (gauss)	7.8 μ Absorption
DS-1	4.1×10^{14}	2.0028	8.3	ND
DS-2	5.1×10^{13}	2.0031	2.1	ND
DS-3	3.4×10^{13}	2.0030	1.0	W
DS-4	---	2.004	1.6	---
DS-5	---	2.0027	0.3	FS

Notation: ND - not detected
W - weak
FS - fairly strong for semiconducting diamonds.

The g-factor was found to be independent of the orientation of the diamonds in the applied magnetic field. In addition, as noted in Table IV, the value of the g-factor is larger than that for the free electron. The positive g-shift indicates that the resonance absorption may be caused by a defect center containing holes rather than electrons.[5] The g-factor isotropy and the symmetry of the resonance line suggest that the defect center is one of highly symmetrical properties. In the diamond lattice one would expect that such a resonance could originate from an isolated vacancy or from an interstitial atom.

The paramagnetic center described above and characterized by the

[5]The criterion of attributing a positive g-shift to holes must be used with caution. See reference (61) for further comments, p. 214.

properties outlined in Table IV is quite similar to the resonance line found in neutron-irradiated diamond (22). The most prominent feature of the ESR spectrum in neutron-irradiated diamond is a single isotropic line with a g-factor equal to 2.0028. The line width in neutron-irradiated diamond for 10 hours exposure was 20 gauss. Both the intensity and line width increased with increased irradiation time but were found to decrease rapidly upon heating the diamond. In experiments on crushed diamond we have obtained a g-factor of 2.0029 for a single resonance line; furthermore, the intensity and line width decreased on heating the crushed diamond above 500°C. Therefore, in irradiated and crushed diamond it is thought that the single resonance line is due to the paramagnetism associated with generated vacancies.

In addition to the ESR measurements, it is possible to estimate the number of acceptors responsible for the p-type conductivity of DS-1 and DS-2. From the measured resistivity of these semiconducting diamonds and using a hole mobility of 1300 cm^2/volt-sec (48), a calculation yields the following number of acceptors (N_A):

Diamond	N_A
DS-1	1×10^{14}
DS-2	6×10^{13}

Comparing the number of acceptors with the number of spins in Table IV shows an extremely fortuitous result that appears to be significant in analyzing the electronic properties of semiconducting diamonds. Thus, with the above information, it is considered highly probable that the electron spin resonance signal is due to the acceptor center in p-type diamonds, and the unpaired spin of the hole is located at a vacancy in the diamond

lattice.

It is interesting to note at this point that the irradiation of diamond with electrons and neutrons has not produced any semiconducting diamonds, although the conductivity of natural semiconducting diamonds is usually reduced upon irradiation (62).

Perhaps the most interesting characteristic of the ESR line in semiconducting diamond is the decrease of the line width as the infrared absorption at 7.8 μ increases. In order to explain this particular feature it is assumed that donors are present and that a small degree of compensation occurs. The occurrence of both acceptors and donors in these diamonds is consistant with Hall data (48). The 7.8 μ absorption band is considered to be a measure of the number of uncompensated acceptors. Therefore, as the 7.8 μ absorption increases the intensity of the ESR signal should decrease. Table IV shows that this is the case for DS-1 and DS-3. The nature of the donors is not known; however, nitrogen is known to be a common donor in diamonds.

The ESR line may also be narrowed through the mechanism of an exchange interaction via the compensated acceptor. The exchange narrowing of a resonance line depends critically on the magnitude of overlap of the wave functions belonging to the respective spin centers (63). Exchange narrowed lines have a characteristically narrow central portion with broad wings on the resonance curve. In principle, the exchange interaction should be effected by the process of compensation in semiconductors containing both donors and acceptors. The presence of an electron at an acceptor center has the effect of attracting the positively charged holes and to increase the overlap of the wave functions of the spin centers closest to the compensated center. This mechanism of line narrowing could account for the

decreased line widths in the diamonds DS-3 and DS-5. The 7.8 μ absorption occurs in the semiconducting diamonds where compensation is present, and is due to the excitation of an electron from a compensated to an uncompensated acceptor site.

Concerning the ESR Absorption in Insulating Diamonds

In addition to the studies on semiconducting diamonds, the ESR absorption spectra of several insulating diamonds was investigated. The diamonds studied included both Type I and Type IIa. Most of the diamonds showed ESR absorption, with the more complex spectra being observed in colored diamonds. Several diamonds among the 67 in the Oklahoma State University collection are of interest; in particular, a series of five diamonds which have a cubic growth habit and show the ESR hyperfine spectrum generally attributed to nitrogen. Some of the diamonds have the same fine yellow color but have different ESR spectra, with measurable differences in their infrared and birefringence properties. A relatively simple 3-line ESR spectrum occurs in a yellow diamond exhibiting little or no birefringence and no infrared absorption at 7.3 μ; whereas, a more complex spectrum is observed in the other yellow diamonds with these properties. A complete study of the resonance spectra in colored diamonds was not attempted in this investigation.

ESR Spectrum of Nitrogen in Diamond

The spin I of the nitrogen isotope N^{14} is equal to 1, and the natural abundance is about 99.6%. Thus, the ESR spectrum of atomically dispersed N^{14} in the diamond lattice would be expected to consist of one or more sets of three equally intense hyperfine lines. For the nitrogen resonance in diamond there are four types of impurity centers with the symmetry axis

along ⟨111⟩ directions (21). In case the magnetic field is parallel to the ⟨100⟩ direction a three-line spectrum similar to Figure 4-6c is obtained. This nitrogen resonance has been detected in five diamonds exhibiting a cubic growth habit. In addition, the infrared spectra of D-66 shown in Figure 4-8 is characteristic of these cubes. Several absorption lines occur in the region around the peaks at 3.2 and 7.1 μ. The absorption at 7.3 μ, which is usually found in yellow diamonds, is absent in the diamond cubes (D-62, 63, 64, 65, and 66), as well as D-51B. In diamonds where the 7.1 μ band may be covered by strong absorption in that region, the absorption peak at 3.2 μ can be readily distinguished if the absorption center is present.

In a particular diamond, D-51B, the measured intensity ratio of the three-line spectrum of Figure 4-6c is 1:2:1 rather than 1:1:1 as one would expect for the nitrogen resonance. The 1:2:1 ratio could result from an unpaired spin located at a carbon atom on which two hydrogen atoms are attached, but no further proof of this model was obtained. Since no correlation between the nitrogen resonance intensity and the infrared absorption at 7.8 μ has been found, it is possible that the infrared absorption at 3.2 μ and 7.1 μ (see Fig. 4-8) may be associated with the ESR signal in the diamond D-51B.

Complex ESR Spectrum in Type I Diamonds

The complex ESR absorption thatis observed in several Type I diamonds of various colors (brown, yellow, and green) appears to arise from the overlapping of at least two spectra. The complex spectra appear in these diamonds in conjunction with infrared absorption at 7.3 μ.

A green diamond (D-57) has the ESR absorption spectrum of Fig. 4-5.

D-57 shows no infrared absorption at 3.2 μ, as shown in Fig. 4-8, and does not have the ESR lines split off by 34 gauss from the central group which are observed in D-52A and D-55. Also, one should note the apparent collapse of the hyperfine lines into a single line when the magnetic field is parallel to the ⟨110⟩ direction.

The complex spectrum is found in a yellow-green diamond (D-52 A) but with different orientation dependence and additional lines. The collapse of the hyperfine structure in this diamond occurs when the magnetic field is approximately parallel to the ⟨111⟩ direction. An investigation of the infrared absorption shows a small peak at 3.2 μ (Fig. 4-9). In addition, there are ESR lines occurring at approximately 34 gauss from the central group.

The ESR spectrum of a brown diamond (D-61) is shown in Fig. 4-7. The prominent feature of the resonance curve in this diamond is the sharp line superimposed upon the complex spectrum and the occurrence of lines when the ⟨100⟩ direction is parallel to the magnetic field. The side lines are separated from the center by about 35 gauss and disappear when the magnetic field is parallel to the ⟨110⟩ direction. The particular defect giving this type of resonance has a symmetry axis parallel to the ⟨110⟩ direction. There was no significant difference in the infrared spectrum of D-61 and D-57, although D-61 is brown and D-57 is green. Both diamonds show strong infrared absorption at 7.3 μ as shown by Fig. 4-8.

The resonance spectrum of diamond D-55 is not shown, but this diamond has a complex spectrum with side peaks. In the infrared D-55 shows, what might have been predicted from the ESR spectra, absorption at 3.2, 7.1, and 7.3 μ.

Summary and Conclusions

ESR in Semiconducting Diamonds

The electron spin resonance absorption in semiconducting diamonds was found in this investigation to be associated with the acceptor center in the p-type diamonds studied. Five semiconducting diamonds were available for study, and experimental results were obtained on the g-factor, line width, and the number of unpaired spins contributing to the resonance. The g-factor and number of unpaired spins are two of the measured parameters used to identify the spin center as an acceptor site. The g-factor in all the semiconducting diamonds is close to the value 2.0030; the positive g-shift from the free electron value of 2.0023 may be associated with the electronic state corresponding to a hole rather than an electron (58). In addition to the positive g-shift, the number of unpaired spins was found to agree quite closely with the determined number of acceptors in two of the semiconducting diamonds investigated. The temperature variation of the magnetic susceptibility was measured , and it was found to follow the Curie law from $108^{o}K$ to $370^{o}K$.

The width of the resonance line varies from 0.3 to 8 gauss for different semiconducting diamonds at room temperature. The diamond having the more narrow line width, 0.3 gauss, exhibited a fairly strong infrared absorption at 7.8 μ. The 7.8 μ infrared absorption is assumed to be influenced by the degree of compensation; i.e., a stronger absorption at 7.8 μ would indicate a larger concentration of donors which could supply electrons for the compensation of the acceptor centers. The compensation of acceptor spin centers by electrons would have the effect of diluting the spin concentration and, if dipolar broadening is predominant, would

effectively narrow the resonance line. Also, if the concentration of spins is large or compensation is present, the mechanism of exchange narrowing could be effective in reducing the line width. Dipolar broadening probably makes the major contribution to the line width of DS-1 which is 8 gauss. The width of the resonance line in DS-2 is 2.7 gauss and, since the 7.8 μ band is absent in the diamond DS-2, the reduced line width could be due simply to the smaller concentration of acceptor spins. The narrower lines of DS-3 and DS-5, with the occurrence of the infrared absorption at 7.8 μ, indicate that compensation of the acceptors by available donors is present. The resonance lines are narrowed by the exchange interaction between spins located near a compensated acceptor. In addition, the spin-lattice interaction contributes to the line width in these diamonds. Saturation measurements could not be made; however, an estimate of the spin-lattice relaxation time of 10^{-9} seconds was obtained. The line width is isotropic with respect to the orientation of the magnetic field.

The measurements at liquid helium temperature include the determination of the g-factor (g=2.01) and the resolution of the hyperfine structure, which is presumed to be due to the interaction with the C^{13} nuclei.

The experimental results suggest that the acceptor spin center is a vacancy in the diamond lattice. Although the exact distribution of the acceptors remains uncertain, it is possible that the defects responsible for the p-type conductivity lie in thin layers parallel to the (111) plane. The high concentration of spin centers in the impurity layers could partially account for the measured line widths in the semiconducting diamonds. Simple considerations of the line width indicate that the acceptor density is probably as high as 10^{21} per cc in impurity layers, with the thickness of the layer being of the order of 100 - 1000 Å.

In summary, the following conclusions derived from the present investigation on electron spin resonance seem important in describing the electronic levels in semiconducting diamonds:

(1) The spin resonance absorption is associated with the acceptor center in p-type diamonds.

(2) The acceptor center is probably associated with a vacancy.

(3) The acceptor defects are distributed in thin layers that lie on (111) planes.

(4) The concentration of acceptors may be as high as 10^{21} per cc.

(5) Exchange interaction between acceptors is possible via the compensation of acceptors.

ESR and Infrared Studies of Type I Diamonds

Diamonds that are colored usually have a complex ESR spectrum which is difficult to analyze because of overlapping lines. The orientation dependence of the observed 13-line spectrum is complicated and apparently variable from specimen to specimen. Studies of the infrared absorption indicate that the 7.3 μ peak (B center) is associated with the defect center responsible for the complicated ESR spectrum in colored diamonds. It is possible that impurity-defect association or impurity clustering is present in these diamonds to give the observed ESR and infrared spectra.

The unusual spectrum observed in a brown diamond (D-61) could be associated with the $\langle 110 \rangle$ luminescent center studied by Elliott, et. al., (65). The defect center could possibly involve a vacancy and an impurity; the model they suggest involves a vacancy bound to an impurity in a next-nearest-neighbor position.

The usual nitrogen resonance is observed in a series of diamond cubes;

however, an unusual 3-line spectrum was obtained in a clear yellow diamond with an intensity ratio of 1:2:1 when the ⟨100⟩ direction is parallel to the magnetic field. A plausible explanation could include the possibility of the interaction of the unpaired electron with two hydrogen atoms attached to a carbon atom. Associated with the 3-line ESR spectrum is the infrared absorption at 3.2 and 7.1 μ.

Suggestions for Further Study

The results of the present investigation suggest several possibilities for further research on the electron spin resonance properties of diamond. Future studies should include the following:

(1) A determination of the spin resonance absorption of semiconducting diamonds in the temperature range 4.2°K to 77°K.

(2) Further studies on semiconducting diamonds in the range 1.3°K to 4.2°K.

(3) A study of the effects of monochromatic light on the electron spin resonance spectrum of semiconducting diamond.

(4) Study the ESR spectrum of diamonds under the application of uniaxial stress.

(5) Investigate the temperature dependence of the ESR spectra in colored diamonds.

BIBLIOGRAPHY

1. Ludwig, G. W. and Woodbury, H. H., "Electron Spin Resonance in Semiconductors," Solid State Physics 13, 223 (1962).

2. Kittel, C., Introduction to Solid State Physics, (John Wiley and Sons, Inc., New York, 1959), p. 65.

3. Ingram, D. J. E., Free Radicals as Studied by Electron Spin Resonance, (Butterworths Scientific Publications, London, 1958).

4. Uebersfeld, J., "Spectrometre pour Resonance Paramagnetique," Ann. phys. 1, 395 (1956).

5. Robertson, R., Fox, J. J., and Martin, A. E., "Two Types of Diamond," Phil. Trans. Roy. Soc. London 232A, 463 (1934).

6. Sutherland, G. B. B. M., Blackwell, D. E., and Simeral, W. G., "The Problem of Two Types of Diamond," Nature 174, 901 (1954).

7. Clark, C. D., Ditchburn, R. W., and Dyer, H. B., "The Absorption Spectra of Natural and Irradiated Diamonds," Proc. Roy. Soc. 234A, 363 (1956).

8. Kaiser, W. and Bond, W. L., "Nitrogen, A Major Impurity in Common Type I Diamond," Phys. Rev. 115, 857 (1959).

9. Custers, J. F. H., "Minor Elements in Diamond and Their Effects on Diamond Colors," Gems and Gemology ____, 111 (1957).

10. Custers, J. F. H., "Unusual Phosphorescence of a Diamond," Physica 18, 489 (1952).

11. Custers, J. F. H., "Semiconductivity of a Type IIb Diamond," Nature 176, 173 (1955).

12. Custers, J. F. H., "Type IIb Diamonds," Physica 20, 183 (1954).

13. Stein, H. J., Bell, M. D., and Leivo, W. J., "Optical Studies on Semiconducting Diamond," Bull. Am. Phys. Soc. 1, 127 (1956).

14. Stein, H. J., "Determination of Energy Levels in Semiconducting Diamond by Transmission Methods," (Thesis, Oklahoma State University, 1957) ASTIA-AD-211036.

15. Wentorf, R. H., Jr., and Bovenkerk, H. P., "Preparation of

Semiconducting Diamonds", J. Chem. Phys. 36, 1987 (1962).

16. Sutherland, G. B. B. M., "Some Comments on the Infrared Spectra of Diamond, Silicon, and Germanium," J. Opt. Soc. Am. 50, 1201 (1960).

17. Elliott, R. J., "Speculation on the Centers Formed by Nitrogen in Diamond," Proc. Roy. Soc. 76, 787 (1960).

18. Kemmey, P. J. and Mitchell, E. W. J., "Current Problems in Diamond Physics," Proc. Int. Conf. Semicond. Phys., (Prague, 1960), p. 919.

19. Raal, F. A., "A Spectrographic Study of the Minor Element Content of Diamond," Am. Mineralogist 42, 354 (1957).

20. Evans, T. and Phaal, C., "Imperfections in Type I and Type II Diamonds," Proc. Roy. Soc. 270A, 538 (1962).

21. Smith, W. V., Sorokin, P. P., Gelles, I. L., and Lasher, G. J., "Electron Spin Resonance of Nitrogen Donors in Diamond," Phys. Rev. 115, 1546 (1959).

22. Griffiths, J. H. E., Owen, J., and Ward, I. M., "Paramagnetic Resonance in Neutron-Irradiated Diamond and Smoky Quartz," Nature 173, 439 (1954).

23. Falkner, E. A. and Lomer, J. N., "Electron Spin Resonance in Electron-Irradiated Diamond," Phil. Mag. 7, 1995 (1962).

24. Baldwin, J. A., Jr., "Electron Paramagnetic Resonance Investigation of the Vacancy in Diamond," Phys. Rev. Letters 10, 220 (1963).

25. Falkner, E. A., Mitchell, E. W. J., and Whippey, P. W., "Electron Spin Resonance in Neutron-Irradiated Diamond," Nature 198, 981 (1963).

26. Smith, W. V., Gelles, I. L., and Sorokin, P. P., "Electron Spin Resonance of Acceptor States in Diamond," Phys. Rev. Letter, 2, 39 (1959).

27. Bell, M. D. and Leivo, W. J., "Electron Spin Resonance in Semiconducting Diamond," Bull. Am. Phys. Soc. 6, 142 (1961).

28. Walters, G. K. and Estle, T. L., "Paramagnetic Resonance of Defects Introduced Near the Surface of Solids by Mechanical Damage," J. Appl. Phys. 32, 1854 (1961).

29. Raal, F. A., "A New Absorption Band in Diamond and its Likely Cause," Proc. Phys. Soc. 71, 846 (1958).

30. Bloch, F., "Nuclear Induction," Phys. Rev. 70, 460 (1946).

31. Rabi, I. I., Ramsey, N. F., and Schwinger, J., "Use of Rotating

Coordinates in Magnetic Resonance Problem," Rev. Mod. Phys. 26, 167 (1954).

32. Abragam, A., Principles of Nuclear Magnetism, (Oxford University Press, London, 1961)

33. Garwin, R. L., "Efficient Precision Current Regulator for Low Voltage Magnets," Rev. Sci. Instr. 29, 223 (1958), Erratum: Rev. Sci. Instr. 29, 900 (1958).

34. Johnson, S. D. and Singer, J. R., "Precision Current Regulator using Transistors," Rev. Sci. Instr. 29, 1026 (1958).

35. Garwin, R. L., Hutchinson, D., Penman, S., and Shapiro, G., "Efficient Precision Current Regulator for High Power Magnets," Rev. Sci. Instr. 30, 105 (1959).

36. Montgomery, C. G., Techniques of Microwave Measurements, MIT Radiation Lab Series, Vol. 11, (McGraw-Hill, New York, 1947).

37. Pound, R. V., "Electronic Frequency Stabilization of Microwave Oscillators," Rev. Sci. Instr. 17, 49 (1946).

38. Zaffarano, F. P. and Galloway, W. C., "Notes on the Pound Microwave Frequency Stabilizer," Technical Report #31, Research Laboratory of Electronics, MIT (1947).

39. Stranberg, M. W. P., Tinkham, M., Solt, I. H., Jr., and Davis, C. F., "Recording Magnetic-Resonance Spectrometer," Rev. Sci. Instr. 27, 596 (1956).

40. Torrey, H. C. and Whitmer, C. A., Crystal Rectifiers, MIT Radiation Lab. Series, Vol. 15, (McGraw-Hill, New York, 1947).

41. Karplus, R., "Frequency Modulation in Microwave Spectroscopy," Phys. Rev. 73, 1027 (1948).

42. Gordon, J. P., "Variable Coupling Reflection Cavity for Microwave Spectroscopy," Rev. Sci. Instr. 32, 658 (1961).

43. Feher, G., "Sensitivity Considerations in Microwave Paramagnetic Resonance Absorption Techniques," Bell System Tech. J. 36, 449 (1957).

44. Faulkner, E. A., "Improved Circuit for an Electron Spin Resonance Spectrometer," J. Sci. Instr. 39, 135 (1962).

45. Singer, J. R. and Johnson, S. D., "Transistorized Nuclear Resonance Magnetic Field Probe," Rev. Sci. Instr. 30, 92 (1959).

46. Buss, L. and Bogart, L., "Wide Range Marginal Oscillator for Operating Nuclear Resonance Probes through Flexible Cable," Rev. Sci. Instr. 31, 204 (1960).

47. DuMond, J. W. M. and Cohen, E. R., Handbook of Physics (McGraw-Hill, New York, 1958), p. 7-170.

48. Leivo, W. J., et al, "Investigation of Semiconducting Properties of Semiconducting Diamond," Report No. AFOSR-2642, (May, 1962).

49. Andrew, E. R., "Nuclear Magnetic Resonance Modulation Correction," Phys. Rev. 91, 425 (1953).

50. Spry, W. J., "Correction for the Finite Magnetic Modulation Amplitude in PMR and NMR Lines," J. Appl. Phys. 28, 660 (1957).

51. McCall, D. W., "Corrections for Nuclear Magnetic Resonance Measurements," J. Appl. Phys. 29, 739 (1958).

52. Burgess, V. R., "Analogue Method for Computing the Number of Spins Contributing to a Magnetic Resonance Absorption," J. Sci. Instr. 38, 98 (1961).

53. Gaffney, John and Clement, J. R., "Liquid Level Finder," Rev. Sci. Instr. 26, 620 (1955).

54. White, G. K., Experimental Techniques in Low-Temperature Physics (Oxford University Press, London, England, 1959), p. 205.

55. Clark, C. D., Kemmey, P., Mitchell, E. W. J., and Henis, B. W., "The Infrared Absorption of Hot Semiconducting Diamonds," Phil. Mag. 5, 127 (1960).

56. Smith, S. D. and Taylor, W., "Optical Phonon Effects in the Infrared Spectrum of Acceptor Centers in Semiconducting Diamond," Proc. Phys. Soc. 79, 1142 (1962).

57. Hyde, J. S., "Magnetic Resonance and Rapid Passage in Irradiated LiF", Phys. Rev. 119, 1483 (1960).

58. Van Wieringer, J. S., Semiconductors and Phosphors, edited by M. Schon and H. Welker, (Interscience Publishers, Inc., New York, 1958), p. 367.

59. Leivo, W. J. and Smoluchowski, R., "A Semiconducting Diamond," Phys. Rev. 98, 1532 (1955).

60. Rauch, C. J., "Millimeter Cyclotron Resonance in Diamond," International Conf. on the Physics of Semiconductors, University of Exeter, 1962.

61. Slichter, C. P., Principles of Magnetic Resonance (Harper and Row, New York, 1963).

62. Kemmey, P. J., "Irradiation of Semiconducting Diamond," Diamant 5, 4 (1962).

63. Pake, G. E., Paramagnetic Resonance (W. A. Benjamin, Inc., New York, 1962).

64. Woodbury, H. H. and Ludwig, G. W., "Electron Spin Resonance Studies in SiC," Phys. Rev. 124, 1083 (1961).

65. Elliott, R. J., Matthews, I. G., and Mitchell, E. W. J., "The Polarization of Luminescence in Diamond," Phil. Mag. 3, 360 (1958).

VITA

Marvin Drake Bell

Candidate for the Degree of

Doctor of Philosophy

Thesis: ELECTRON SPIN RESONANCE IN DIAMOND

Major Field: Physics

Biographical:

Personal Data: Born in Tulsa, Oklahoma, January 14, 1929, the son of George M. and Dana Bell.

Education: Attended grade school in Tulsa, Nowata, and Bartlesville, Oklahoma; graduated from Bartlesville College-High School in 1947; received the Bachelor of Science degree from the Oklahoma State University, with a major in physics, in August, 1955; received the Master of Science degree from the Oklahoma State University, with a major in physics, in August, 1956; completed requirements for the Doctor of Philosophy degree in May, 1964.

Experience: Employed as a draftsman for one year (1951-52); chemist assistant for two years (1952-54); physicist for two years (1956-58); graduate instructor of general physics for three semesters (1958-60).

Organization: Member of American Physical Society, Sigma Pi Sigma, Phi Kappa Phi, and associate member of Sigma Xi.